SLAC-PROPOSAL-E156

March 15, 1997

Proposal to Measure
Polarized Open Charm Photoproduction

R. G. Arnold, P. E. Bosted(*), P. DePietro, D. Reyna, S. E. Rock,

L. Sorrell, T. Toole, Z. M. Szalata

(*) co-spokesperson (contact: BOSTED@SLAC.STANFORD.EDU (415) 926-2319)

The American University, Washington, D.C. 20016

C. Berisso, R. Hicks, G. Peterson, J. Shaw

University of Massachusetts, Amherst, Massachusetts 01003

T. Averett

California Institute of Technology, Pasadena CA

H. Borel*, R. Lombard*, Y. Terrien*

DAPNIA-Service de Physique Nucleaire Centre d'Etudes de Saclay, F-91191 Gif/Yvette, France

(*) *(subject to final approval)*

S. Penttila

Los Alamos National Laboratory, Los Alamos, New Mexico

A. Klein, S. Kuhn, C. Hyde-Wright, L. M. Qin, F. Wesselmann

Old Dominion University, Norfolk, Virginia 23529

T. Marvin

Southern Oregon University, Ashland, Oregon

RECEIVED
MAR 18, 1997

M. Buenerd

Institut de Sciences Nucleaires, Grenoble, France

P. Decowski

Smith College, Northampton, Massachusetts 01063

P. Anthony, H. Dutz, R. Erbacher, R. Erickson, T. Fieguth, R. Gearhart, W. Meyer,
M. Perl, R. Pitthan, S. Rokni, S. St.Lorant, L. Stuart, D. Walz

Stanford Linear Accelerator Center, Stanford, California 94309

S. Bueltmann, C. Cothran, D. Crabb(*), D. Day, E. Frlež, C. Harris, R. Hutchins,
R. Lindgren, J. McCarthy, P. McKee, D. Pocanic, O. Rondon, A. Tobias, H. Zhu

(*) co-spokesperson (contact: DGC3Q@VIRGINIA.EDU (804) 924-6790)

University of Virginia, Charlottesville, Virginia 22901

D. Armstrong, K. Griffioen, P. King

College of William and Mary, Williamsburg, Virginia 23187

H. Band, J. Johnson, R. Prepost

University of Wisconsin, Madison, Wisconsin 53706

Abstract

We propose to measure the asymmetry for polarized photoproduction of charmed quarks from polarized targets in End Station A at SLAC, using a large solid angle muon spectrometer. A quasi-mono-chromatic circularly polarized photon beam will be produced from an oriented diamond crystal. The targets will be longitudinally polarized LiD and NH_3 at a temperature of 0.4 K, centered in a 7 T magnetic field to obtain high polarization. Photoproduction of open charm will be tagged by decays of D mesons into high transverse momentum muons. The L/R asymmetry for producing open charm is closely related to the fundamental polarized gluon spin density $\Delta G(x)$. The asymmetry for single muons will be measured as a function of muon momentum, muon transverse momentum, and photon beam energies with sufficient precision to discriminate among models of $\Delta G(x)$ that differ from each other by as little as 10% in the range $0.1 < x < 0.5$. Significant constraints will be placed on both the shape and magnitude of $\Delta G(x)$ in this x region. The projected errors are significantly smaller than for other experiments that plan to make direct measurements of $\Delta G(x)$. We request four months of data taking at 120 Hz (assuming joint running with PEP II), and one month of checkout time to carry out this proposal.

Contents

I. INTRODUCTION

The spin degree of freedom has, in recent years, opened up a new window into our understanding of nucleon structure and electroweak interactions within the Standard Model. Much of this improvement is due to the availability of the high energy, high current, and highly polarized SLAC electron beam. The fixed target program has, in addition, taken advantage of recent major advances in polarized target technology to make the world's most precise measurements [1–3] of the proton and neutron longitudinal spin structure function g_1.

One of the primary goals of these experiments has been to test QCD through comparisons of data and theory for the integral difference $\Gamma_{BJ} = \int_0^1 [g_1^p(x) - g_1^n(x)]dx$. The theoretical prediction for Γ_{BJ} [4] (known as the Bjorken Sum Rule) is fundamental in QCD, and is quite sensitive to the strong coupling constant α_s evaluated at a scale of order a few GeV. The Standard Model is tested by demanding consistency in values of α_s extracted from the Bjorken integral, with precision measurements at the Z-pole mass scale.

The other major goal of the g_1 experiments has been the determination of spin distributions of quarks and gluons in the nucleon ("what carries the spin?"). A "spin crisis", resulting in numerous theoretical papers, arose when early determinations [5] of $\Delta\Sigma = \Delta u + \Delta d + \Delta s$ were found to be much smaller than expected [where $\Delta f = \int_0^1 \Delta f(x, Q^2)dx$, and $\Delta f(x, Q^2)$ are the individual polarized quark spin distribution functions]. At present, the world average for $\Delta\Sigma$ is approximately 0.3 ± 0.06, much smaller than the relativistic quark model prediction of 0.58 [6]. One explanation for this discrepancy is that the strange sea may be highly polarized, but this depends rather strongly on assumptions of SU(3) symmetry between the beta decays in the baryon octet. In any case, the low value of $\Delta\Sigma$ implies strong gluon contributions via loop and radiative corrections in QCD, expected to be stronger in the polarized case than in the unpolarized case due the triangle diagram axial anomaly [7].

Many authors have made fits to the existing data on g_1 to parameterize the spin distribution function (SDF's) $\Delta u(x)$, $\Delta d(x)$, $\Delta s(x)$, and $\Delta G(x)$. The functions are fit at a

reference scale Q_0, and evolved in Q^2 according to the GLAP equations [8]. The full NLO evolution equation splitting functions and Wilson coefficients for the polarized case have been evaluated recently [9], and fits to the most recent data performed [10,11]. Due to the imprecision of present data, several constraints are placed on the x-dependence (based, for example, on constituent counting rules [12]), and on overall magnitudes (i.e. the Bjorken Sum Rule must be satisfied) in order to reduce the number of free parameters. The result is that the gluon distributions found by various authors differ quite strongly, as can be seen from a representative compilation shown in Fig. 1a. The models for $\Delta G(x)$ are taken from Ref. [12] (solid curve, $\Delta G = \int_0^1 dx \Delta G(x) = 0.7$), Ref. [13] (dashed curve, $\Delta G = 1.7$), Ref. [11] (dotted curve, $\Delta G = 2.3$), Ref. [10] (AR model, dash-dot curve, $\Delta G = 1.1$), and Ref. [10] (OS model, short dash curve, $\Delta G = 1.0$). In Fig 1b, the five models have been divided by a common model for $G(x)$ [12] to display the differences in the mid-x region. The fits have been done at a variety of Q_0^2 scales (from 1 to 10 GeV^2), and using different factorization schemes. Bringing all the models to a common value of Q^2 (such as the charmed mass squared, about 10 GeV^2) and a common factorization scheme (such as $M\bar{S}$) would introduce corrections that are generally smaller than the differences between the models themselves, illustrating that the present data on g_1 allow for a very broad range of fits. In fact, one calculation [14] of $\delta G(x)$ in the context of the MIT Bag Model finds the opposite sign for $\delta G(x)$ than for the models shown in Fig. 1.

Since $G(x)$ and $\Delta G(x)$ fall with x at least as fast as $(1-x)^4$, there is essentially no experimental sensitivity to either $G(x)$ or $\Delta G(x)$ for $x > 0.5$, as can be seen in Fig. 1a. In the region $0.1 < x < 0.5$, it can be seen that present data allow $\Delta G(x)/G(x)$ to be anywhere between 0 and 0.8, and the x dependence of different models varies greatly. Improved data on g_1 from the 50 GeV SLAC experiments E154 and E155, from the lower statistics 1995/1996 SMC data, and from the lower energy HERMES experiment will place additional constraints on the gluon spin, but will likely only reduce the range of acceptable models by a factor of two. This is because the inclusive g_1 measurements do not allow an unambiguous distinction to be made between the sea quark and gluon contributions. In addition, there

could be substantial higher twist contributions to the g_1 data (expected to decrease as $1/Q^2$), which have not been included in the QCD fits because of the difficulty in calculating the x dependence of these contributions (only the first moments have been calculated [15]). With the limited range of Q^2 available in the g_1 data, it will be difficult to distinguish between power law higher twist contributions and the logarithmic gluon contributions to the Q^2 dependence of g_1.

Thus, it is very important to have experiments primarily sensitive to the polarized gluon density. The first such experiment (Fermilab E704 [16]) using polarized proton scattering on a fixed target measured two jet production (from gg collisions) to rule out $\Delta G(x)/G(x)$ as large as 1 at $x \approx 0.15$, but cannot distinguish between models that are between 0 to 0.6 (such as the curves in Fig. 1).

Several methods have been proposed to further study $\Delta G(x)$. An experiment at RHIC [17] plans to look for high transverse momentum photons coming from polarized proton-proton scattering. The kinematics are chosen to emphasize the process $q + g \rightarrow \gamma + q$, and accesses the region $0.05 < x < 0.33$. The statistical precision is expected to give errors on $\Delta G(x)/G(x)$ on the order of 0.01 to 0.3 over this x range. The interpretation is somewhat complicated because contributions for polarized quarks must be carefully taken into account. This program is expected to begin around the year 2000.

The most promising approach to studying polarized gluons in the nucleon is photo- or electro-production of either open charm or inelastic J/ψ's. Since the large ~ 1.5 GeV mass of the charm quark strongly suppresses intrinsic contributions to the nucleon compared to the light quarks, in most kinematic regions the mechanism for observing a pair of charmed quarks in the final state is expected to be dominated by the hard, photon-gluon fusion process $\gamma + g \rightarrow c\bar{c}$ (see Fig. 2). The asymmetry for J/ψ photoproduction has been calculated [18] and is proportional to a ratio of convolution integrals over $\Delta G(x)$ and $G(x)$. Unpolarized J/ψ electroproduction has been used by the EMC and NMC experiments to measure $G(x)$ [19], with kinematic cuts of $z < 0.9$ and $p_t^2 > 1$ GeV^2 to suppress strong contributions from Pomeron exchange. Determining $G(x)$ requires a large normalization factor K that takes

into account higher order processes in the J/ψ formation from the $c\bar{c}$ pair.

Open charm production is more directly interpretable in terms of the photon gluon fusion process [7,18]. In this case the $c\bar{c}$ pair need not be in a color singlet state, and most of the time is produced as a color octet, so a second gluon exchange to the target nucleon is not required. Thus the diffractive Pomeron and the elastic contributions are greatly suppressed relative to the case of J/ψ production. The relatively large charmed quark mass ensures that the relevant momentum transfer scale μ^2 of the problem is of order $\mu^2 = 4m_c^2 \approx 9$ GeV^2, in which case $\alpha_s(\mu^2)/\pi < 0.1$, and perturbative QCD is expected to work reasonably well. Experimentally, open charm has an advantage over inelastic J/ψ photoproduction because the cross section is about 20 times larger , ranging from 60 nb to 200 nb for photons between 20 and 50 GeV, as shown in Fig. 3.

Several proposals have already been made to measure polarized open charm production. The COMPASS [20] group at CERN plans to make measurements with photons with energies between 35 and 85 GeV, and detect open charm principally through various D meson decays. The HERMES experiment at DESY has recently proposed [21] to upgrade their detectors for open charm measurements with photon energies below 27 GeV. There has also been an evaluation of the possibility of using colliding polarized proton and electron beams at HERA (beyond the year 2002) to study polarized open charm production [22]. This would be primarily sensitive to $\Delta G(x)$ at low x.

The following sections give details of our proposal to measure polarized charm photoproduction at SLAC, for photon energies between 13 and 48 GeV. After a brief overview of the photon gluon fusion model, we show the kinematics, backgrounds, rates, and sensitivity of the proposed measurements, followed by a description of the target and detectors. We demonstrate that we expect to make a determination of $\Delta G/G$ with a statistical precision about a factor of ten better than other proposals, and in addition test the reaction mechanism and probe the x-dependence of $\Delta G(x)$ by making measurements in many kinematic bins.

II. POLARIZED OPEN CHARM PHOTOPRODUCTION

A. Introduction

The principal goal of the present proposal is to use polarized open charm photoproduction, tagged by the decays of D mesons into high transverse momentum prompt muons, to learn about $\Delta G(x)$ in the region $x > 0.1$. We first discuss the photon gluon fusion process, which is expected to be the dominant diagram for open charm production. We then explore how the experimental asymmetry in the counting rates for left- and right-handed circularly polarized photons impinging on a longitudinally polarized nucleon target can be related to $\Delta G/G$. Details of how open charm can be tagged using prompt muons are discussed, and reasons given why this method is the best one to use at SLAC, where a high intensity photon beam is available, but with a poor duty cycle. The next subsections deal with the backgrounds, and this section concludes with a comparison of expected error bars with calculations of the asymmetry made with a variety of models of $\Delta G(x)$.

B. The Photon Gluon Fusion Diagram

The dominant mechanism for production of heavy quarks from photon-nucleon interactions is the photon-gluon fusion diagram shown in Fig. 2. The spin-averaged experimental cross section is given by an integral over the product of the elementary photon-gluon cross section $\sigma(\hat{s}, \cos(\theta^*))$ with the gluon distribution $G(x, Q^2)$ [23] and the experimental efficiency $\epsilon(\hat{s}, \cos(\theta^*))$

$$\sigma_{\gamma p}(k) = \int_{x_{min}}^{1} G(x, Q^2) dx \int_{-1}^{1} \sigma(\hat{s}, \cos(\theta^*))\ \epsilon(\hat{s}, \cos(\theta^*))\ \beta\ d\cos(\theta^*) \qquad (1)$$

where k is the photon energy, $x_{min} = 4m_c^2/2Mk$, m_c is the charmed quark mass of about 1.5 GeV, M is the nucleon mass, $s = 2Mk + M^2$ is the square of the c.m. energy in the photon-nucleon system, $\beta = \sqrt{1 - 4m_c^2/\hat{s}}$ is the c.m. velocity of the charmed quark, $\hat{s} = xs$ is the square of the c.m. energy in the photon-gluon system (or the $c\bar{c}$ system), Q^2 is the

momentum transfer squared to the gluon (taken in our calculations to be $Q^2 = \hat{s}$), θ^* is the c.m. angle of the charmed quarks, and

$$\sigma(\hat{s}, \cos(\theta^*)) = \frac{4}{9}\frac{2\pi\alpha\alpha_s(\hat{s})}{\hat{s}}\left[\frac{-8m_c^4\hat{s}^2}{\hat{t}^2\hat{u}^2} + 2\frac{\hat{t}^2 + \hat{u}^2 + 4m_c^2\hat{s}}{\hat{t}\hat{u}}\right] \tag{2}$$

where $\hat{t} = \frac{\hat{s}}{2}[1 + \beta\cos(\theta^*)]$, and $\hat{u} = \frac{\hat{s}}{2}[1 - \beta\cos(\theta^*)]$. For small β ($\hat{s} < 15$ GeV^2), $\sigma(\hat{s}, \cos(\theta^*))$ is approximately independent of $\cos(\theta^*)$, and the integrated form

$$\sigma(\hat{s}) = \frac{4}{9}\frac{2\pi\alpha\alpha_s(\hat{s})}{\hat{s}}\left[-\beta(2 - \beta^2) + \frac{1}{2}(3 - \beta^4)\ln\frac{1+\beta}{1-\beta}\right]. \tag{3}$$

can be used.

The charmed quarks undergo the fragmentation process once they are produced, with the result that, on average, a little less than two D mesons are produced per $c\bar{c}$ pair. Occasionally, Λ_c and η_c are observed in the final state as well (see Table I).

The total cross section for this process has been fairly well measured [24] and averages about 170 nb for photons between 39 and 48.5 GeV. The transverse momentum (p_T) dependence of the D mesons is exponential and falls as $d\sigma/dp_T^2 \approx e^{-p_T^2/<p_T^2>}$, with a mean value of $< p_T^2 > \approx 1$ GeV^2. The distribution in x_F is approximately Gaussian with a mean value of 0.2 and a width of 0.5. NLO corrections have been calculated, and change the total cross section by about 35%, but have little effect on the p_T and x_F distributions. The magnitude of the cross section, the x_f dependence, and the p_T dependence are in very good agreement with predictions from the photon-gluon fusion process, using gluon distributions determined from other reactions [24].

For polarized photons and longitudinally polarized nucleons, the polarized experimental cross section component $\Delta\sigma_{\gamma p}(k)$ is given by [18]

$$\Delta\sigma_{\gamma p}(k) = \int_{x_{min}}^{1} \Delta G(x, Q^2)dx \int_{-1}^{1} \Delta\sigma(\hat{s}, \cos(\theta^*))\ \epsilon(\hat{s}, \cos(\theta^*))\ \beta\ d\cos(\theta^*) \tag{4}$$

where

$$\Delta\sigma(\hat{s}, \cos(\theta^*)) = \frac{4}{9}\frac{2\pi\alpha\alpha_s(\hat{s})}{\hat{s}}\left[\frac{4m_c^4(\hat{t}^3 + \hat{u}^3)}{\hat{t}^2\hat{u}^2} + 2\frac{\hat{t}^2 + \hat{u}^2 - 2m_c^2\hat{s}}{\hat{t}\hat{u}}\right]. \tag{5}$$

Integrated over $\cos(\theta^*)$, this becomes

$$\Delta\sigma(\hat{s}) = \frac{4}{9}\frac{2\pi\alpha\alpha_s(\hat{s})}{\hat{s}}\Big[-3\beta + \ln\frac{1+\beta}{1-\beta}\Big]. \tag{6}$$

This is a reasonable approximation for $\hat{s} < 15$ GeV^2, as can be seen in Fig. 4, where $\sigma(\hat{s}, \cos(\theta^*))$ and $\Delta\sigma(\hat{s}, \cos(\theta^*))$ are plotted versus $\cos(\theta^*)$ over the range from 0 to 1 (-1 to 0 is mirror symmetric). Although $\sigma(\hat{s}, \cos(\theta^*))$ is relatively slowly varying, $\Delta\sigma(\hat{s}, \cos(\theta^*))$ changes sign for $\hat{s} > 20$ and $|\cos(\theta^*)| < 0.8$, so it is important to include the experimental efficiency $\epsilon(\hat{s}, \cos(\theta^*)$ when evaluating the total polarized counting rate for a given kinematic setting. The best sensitivity comes from an experimental efficiency that emphasizes mostly positive or negative $\Delta\sigma(\hat{s}, \cos(\theta^*))$. On the other hand, kinematics that emphasize the transition through zero are less sensitive to ΔG, but test the underlying reaction mechanism.

C. Experimental asymmetry for open charm

For a mono-chromatic photon beam, the ratio of $\Delta\sigma_{\gamma p}(k)/\sigma_{\gamma p}(k)$ is directly proportional to the experimental asymmetry

$$A_{cc}(k) = \frac{1}{P_t P_b f}\,\frac{N^{\uparrow\uparrow} - N^{\downarrow\uparrow}}{N^{\uparrow\uparrow} + N^{\downarrow\uparrow}} = \frac{\Delta\sigma_{\gamma p}(k)}{\sigma_{\gamma p}(k)} \tag{7}$$

where P_t is the target polarization, P_b is the photon beam polarization, and f is the target dilution factor (fraction of polarizable nucleons). The rates of detected muons normalized to the incident beam flux for parallel and anti-parallel spins are denoted by $N^{\uparrow\uparrow}$ and $N^{\downarrow\uparrow}$.

By measuring the asymmetry A_{cc}, the sensitivity to common factors (such as the scale at which $\alpha_s(\mu^2)$ is evaluated, the charm quark mass, or the branching ratios for D decays to muons) cancel out, reducing the theoretical uncertainty. Additional uncertainties remain from higher order QCD diagrams. The NLO polarized open charm cross section is presently being calculated by three groups, but is not yet available to us. There is the possibility that polarization dependence in the fragmentation process could change the kinematics of the produced D mesons and their decay muons. We minimize this effect by averaging over both muon signs and a large range of kinematics.

For a continuous-energy-distribution photon beam (such as bremsstrahlung), the experimental asymmetry depends on the ratio of integrated predicted experimental rates:

$$A_{cc}(E) = \frac{1}{P_t P_b f} \frac{N^{\uparrow\uparrow} - N^{\downarrow\uparrow}}{N^{\uparrow\uparrow} + N^{\downarrow\uparrow}} = \frac{\int_0^E D(k)\Phi(k)\Delta\sigma_{\gamma p}(k)}{\int_0^E \Phi(k)\sigma_{\gamma p}(k)} \tag{8}$$

where the photon flux $\Phi(k) \approx \frac{(t/X_0)}{k}$ for bremsstrahlung from an amorphous material, where t is the thickness of a radiator with radiation length X_0 through which the electron beam passes, and the depolarization factor is $D(y) \approx [1-(1-y)^2]/[1+(1-y)^2]$, where $y = k/E$, and E is the photon endpoint energy (the energy of the primary electron beam). As discussed in more detail below, we plan to use bremsstrahlung from a diamond crystal, oriented to give a large enhancement of the flux at high photon energies, compared to the incoherent flux characteristic of amorphous materials.

We plan to detect D mesons by their semi-leptonic decays to muons. Since large p_T muons are strongly correlated with even higher p_T D mesons, the average $x = \hat{s}/s$ of the gluon probed increases with the p_T of the muon. This is because large p_T charmed mesons are correlated with large $\sqrt{\hat{s}}$, by conservation of momentum.

D. Tagging Open Charm with Single Muons

We have simulated open charm production using the PYTHIA 5.7 Monte Carlo [25] run in photoproduction mode, with only the process of open charm creation by the photon-gluon fusion mechanism turned on. The spin-averaged LO QCD cross section given above is used, with the $G(x, Q^2)$ taken from a CTEQ fit, yielding the curve shown in Fig. 3. The JETSET portion of the Monte Carlo takes care of the fragmentation process to generate a pair of charmed hadrons, which then decay using the known branching ratios. The decays to muons are not nearly as well measured at present as those to electrons, so the very reasonable assumption has been made that muon and electron semi-leptonic branching ratios are equal. The result is that about 24% of all open charm events have at least one prompt muon in the final state. These come about equally from charged and neutral D's, since charged D's

are twice as likely to decay to muons, but are only produced about half as often, with the next biggest source being Λ_c. Table I shows the number of each type of parent particle from which a muon with $p_T > 0.5$ GeV and momentum $P_\mu > 3$ GeV originated (assuming an average of 25 cm allowed for pions and kaons to decay). The parents of the pions and kaons are mostly the light D mesons, while the τ parents are always the heavier D_s. A quark momentum distribution parameter in PYTHIA was adjusted to give agreement with the charm/anti-charm asymmetry measured in Fermilab E687 [26]. Note that there are quite a lot of Λ_C produced by associated production: the fraction of such final states increases as the photon energy is lowered, in agreement with the 20 GeV photon bubble chamber measurements made at SLAC [27]. Since the Λ_C is considerably less likely to decay to a muon than the D mesons are, the model predicts an excess of μ^- over μ^+, with the excess increasing at lower energies. Fortunately, this is opposite to the trend from the background of decays of pions and kaons to muons, discussed in more detail below.

The average muon momentum from open charm events is about 3 GeV, and the average p_T is about 0.4 GeV, extending with significant counting rate to as high as 2 GeV. Figure 5a shows (open circles) the number of muons expected from open charm, as a function of p_T, for muons with momenta between 5 and 10 GeV for the high energy component ($k > 42$ GeV) of a coherent photon beam produced by a 48.5 GeV electron beam passing through a 0.07% r.l. diamond radiator at an angle of 5 mr. The number of counts in each p_T bin of 0.1 GeV is for 60 hours of full efficiency running at 120 Hz, an electron current of 1×10^{11} electrons/spill, a 5 gm/cm^2 LiD target, and assuming 100% muon detection efficiency. The photon flux calculation includes the effects of collimation discussed in more detail below. For this luminosity, the number of tagged open charm events per 0.1 GeV p_T bin ranges from a few thousand at very high transverse momentum, to close to a million events at $p_T = 0.5$. The rates are even larger at lower p_T, but the backgrounds become very large (see next section). The rates are higher for muons with $P_\mu < 5$ GeV, but fall faster with p_T, while the reverse is true for muons with $P_\mu > 10$ GeV.

In order to obtain the charm asymmetry at 45 ± 3 GeV, we will need to account for

the incoherent bremsstrahlung contributions. These are shown in Fig. 5b for the design luminosity. To save time, this spectrum would actually be measured using a thicker (0.2% r.l.) amorphous radiator, and running for about 30% of the time used for the diamond radiator. The actual experimental rates of muons would therefore be the sum of Fig. 5a and 5b, which is shown in Fig. 5c.

The kinematic selectivity of the muons is illustrated in Fig. 6. The distribution in $x = \hat{s}/s$ versus $|\cos(\theta^*)|$ for the open charm counts in the second lowest p_T bin of Fig. 5c ($0.6 < p_T < 0.7$) is shown in Fig. 6b. The distribution is very similar to that for the average of all $c\bar{c}$ events generated, shown in Fig. 6a, so that the average x is about 0.15. On the other hand, the events in Fig. 6c for $p_T > 1.0$ come from smaller values of $|\cos(\theta^*)|$, but larger values of x than the average $c\bar{c}$ event, and so preferentially select the region where $\Delta\sigma(\hat{s}, \cos(\theta^*))$ is small and changing sign. Figure 6d shows the distribution for lower p_T muons ($0.6 < p_T < 0.7$) that have high momentum ($15 < P_\mu < 20$ GeV). In this case there is a strong selection towards large values of $|\cos(\theta^*)|$, which means the average value of $\Delta\sigma(\hat{s}, \cos(\theta^*))$ will be more negative than for lower momentum muons with the same transverse momentum.

E. Other Open Charm Tags

We have made a detailed study of the more traditional method of tagging open charm by the two- or three-body decay of D into pions and kaons. The best signal comes from $D^* \to \pi D^0 \to \pi K$, which gives a double kinematic constraint (the masses of the D^0 and D^*) which eliminates most combinatoric background. However, the poor duty cycle at SLAC combined with the large flux of pions and kaons that don't come from charm events limits the usable luminosity to about three orders of magnitude less than if muons are used to tag open charm. The result is that it would take much more running time to get the same error bar on A_{cc}, and the detector apparatus would be much more complicated.

We also investigated using muon pairs (one from each charmed quark) to tag open

charm. The signal is greatly reduced after placing cuts needed to eliminate backgrounds, so the asymmetry errors are about five times larger than using single muons. Since the detector is designed to have good efficiency over a large solid angle, we will register the two muon signal in any case, and it will provide a systematic check on the single muon results.

F. Backgrounds

Although the open charm cross section is only about 0.2% of the total photoproduction cross section at 48.5 GeV, processes other than open charm rarely generate prompt muons, making the signal of one or more high transverse momentum muons a good signature for open charm. This allows us to take advantage of the high luminosity available at SLAC.

1. Pion and Kaon Decays

There are several sources of backgrounds that can generate single muons. The largest is the decay of pions and kaons. We propose to minimize this contribution by placing a copper absorber as close as possible to the target. Assuming that, on average, muon decays occur in the first absorption length (14 cm), and that the target to absorber distance is $[5+0.5/\sin(\theta)]$ cm, we have calculated the flux of muons from pion and kaon decays, represented by the diamond symbols in Fig. 5a,b,c. The approximation that all decays occur in the first 14 cm of copper was checked using GEANT simulations. We have done the hadron flux calculations two ways, and they are in reasonably good agreement (within 30% of each other). The first method was to use PYTHIA, with all photoproduction processes turned on, to generate pions and kaons and keep those that decay within a distance $[20+0.5/\sin(\theta)]$ cm. An average was taken over proton and neutron targets, and the result scaled by 0.7 to account for nuclear shadowing in the predominant lithium component of the target (assuming inclusive photoproduction at moderate p_T scales as $A^{2/3}$). The second method was to use the parameterization of inclusive pion and kaon photoproduction of Wiser [28], which is fit to data at endpoint energies of 5 to 19 GeV. The extrapolation of the Wiser fit to 48.5 GeV

is very close to the PYTHIA rates for π^+, π^-, K^-, but is about a factor of two higher for K^+, approximately independent of p_T. The rates in Fig. 5 are for the sum of μ^- and μ^+: if only μ^- is considered, the ratio of open charm signal to decay background is 1.5 to 4 times larger than if only μ^+ are considered. Thus the consistency of the open charm asymmetry extracted separately from μ^- and μ^+ will be a good check on the systematics of subtracting the decay backgrounds.

As a check on our calculations, we have compared the Wiser and PYTHIA predictions for inclusive negative hadrons to the cross sections measured in inclusive electroproduction from a glass/helium target in SLAC experiment E154. The calculations assume that electroproduction at an endpoint energy of 48.5 GeV is equivalent to photoproduction using a 3.5% radiator, and we make a shadowing correction of $\sim 50\%$ to the nucleons in the glass portion of the target. As can be seen in Fig. 7, the calculations match the p_T dependence of the data extremely well at the two angles measured, and the magnitude is within 20% of the data.

As seen in Fig. 5c, the pion and kaon decays are the largest source of background. As was pioneered in a SLAC experiment in 1975 [29], we plan to measure the relative prompt and decay rates by varying the distance of the absorber from the target. In that 1975 SLAC experiment, this technique was used to measure the prompt rate of muons with $P_\mu = 6$ GeV and $p_T = 1$ GeV at photon endpoint energies of 8, 12, and 20 GeV. The decay rates were found to be in good agreement with a prediction based on the Wiser fit. After correcting for the expected Bethe-Heitler prompt signal, no excess was seen at endpoint energies of 8 and 12 GeV (which are below the $D\bar{D}$ threshold), but a substantial excess was seen at 20 GeV, consistent with that expected from open charm. By measuring both rates and asymmetries as a function of decay distance, we can determine the relative cross sections of prompt and decay muons, as well as their asymmetries.

Fortunately, the evidence of recent experiments E143 and E154 suggests that asymmetries from inclusive photoproduction of hadrons are very small and independent of p_T. The average negative hadron asymmetry for a proton target in E143 was about 0.015 ± 0.005

(corrected for target and electron beam polarization and dilution factor), while for the deuteron target the asymmetry was found to be about -0.010 ± 0.005. The E154 experiment [30] had much better statistics, and found for a neutron target an average asymmetry of -0.012 ± 0.003 for negative hadrons and -0.025 ± 0.005 for positive hadrons (which includes pions, kaons, and a substantial number of protons). All of these asymmetries are much smaller than the expected open charm asymmetry of 0.1 to 0.4, so that systematic errors from decay asymmetries will be minimal.

2. Bethe-Heitler Muon Pair Production

The second class of backgrounds is Bethe-Heitler (BH) muon pair production, in which a photon splits into a muon pair, and one of the muons scatters either a) elastically from a nucleus; b) quasi-elastically from a nucleon; or c) inelastically from a quark. The cross section for BH production is exactly calculable using the formulas of Tsai [31] as long as the form factors F_1 and F_2 are known for each of a), b), and c). From our work in calculating radiative corrections to deep inelastic electron scattering, we have good models for these form factors, and believe the resulting cross section calculations are good to better than 10%. To generate BH events with the proper weighting, we modified a Monte Carlo code (which embodies Tsai's formulas) developed at Fermilab [32], to include process c), and checked the results against the tables shown in Tsai's article. As can be seen in Fig. 5, there are a substantial number of events from the BH process at high p_T, dominated by inelastic scattering. We assumed the target is LiD: using a higher Z target results in a larger signal from process a), which scales as Z^2. We note that the ratio of BH to charm events at fixed p_T increases with muon momentum: this is opposite to the trend for pion and kaon decay muons, where the relative background decreases with P at fixed p_T.

To reduce the BH background, we plan to veto events in which a second, opposite sign, muon is detected (since BH muons are always created in opposite sign pairs). For the detector acceptance, discussed in more detail below, this removes 50% to 80% of the events,

depending on kinematics. The true charm signal is only reduced by a few percent, since the vast majority of charm events result in only a single detected muon. An additional 2% of the charm signal is removed by a random time coincidence with a second, unrelated muon, assuming an approximate rate of 2 opposite sign detected muons/spill for a spill length of 250 nsec, and a veto time bin of 2 nsec. The results are shown in Fig. 5, where it can be seen that in most cases BH/charm is less than 0.1. We can correct for the un-vetoed BH events using the Tsai formulas for the rates, and formulas which still need to be worked out (but should depend on the known structure functions g_1 and g_2) for the asymmetries. We will be able to check the accuracy of the BH asymmetry formulas by comparing with events tagged with opposite sign muons that preferentially come from the BH process ($1.2 < M_{\mu\mu} < 2.5$ GeV, $p_{T\mu\mu}^2 < 0.1$ GeV^2).

We calculated the BH rate for τ lepton pairs, which are produced at large p_T due to their heavy mass of 1.8 GeV. Taking into account the 17% probability for a τ to decay to a muon, we find the background from this source to be less than 1% of the open charm signal.

3. Decays of Light Vector Mesons

We have also considered prompt background from the decays of η, $\rho(770)$, $\omega(782)$, and ϕ mesons, as generated by PYTHIA (star symbols in Fig. 5). The decays into opposite sign muon pairs have small branching ratios (3.1×10^{-4}, 4.6×10^{-5}, 9.6×10^{-5}, and 2.5×10^{-4}, respectively), but they are copiously produced by the soft (low p_T) Vector Dominance mechanism, in which a photon fluctuates into a vector meson and scatters hadronically from a nucleon. Because this is a low p_T process, and because the muons typically acquire an additional p_T of less than half the parent mass, the distribution of vector meson decays falls much more rapidly with p_T than the open charm signal, and will result in a very small correction to the measured asymmetries.

4. Decays of J/ψ

The final background we have considered is muons from J/ψ's, which decay 7% of the time to two opposite sign muons with typical transverse momentum of 1.5 GeV/c. The PYTHIA model treats diffractive production fairly well, but probably has underestimated the inelastic contribution. No J/ψ events show up on the plots of Fig. 5 when the two-muon events are vetoed. If a conservative muon detection efficiency of 0.9 is used instead of the 100% assumed, the J/ψ background remains negligible below p_T of 1.2 GeV/c. If all events with one or more muons are kept (no two-muon veto), a significant contamination of the open charm signal would occur, but only above p_T of 1.1 GeV/c, where the open charm cross section is dropping rapidly.

G. False Asymmetries

As in previous SLAC experiments, we will flip the spin direction of the electron beam (and hence the photon beam) on a random pulse-to-pulse basis. This eliminates false asymmetries due to slow drifts in parameters such as the target polarization or the detector efficiency. Effects due to slight differences in beam parameters (size, emittance, intensity) for the different helicities will be canceled out by periodically reversing the target polarization direction. This will cancel out the parity violating asymmetry for open charm production through Z exchange to unpolarized nucleons. Any remaining false asymmetries have been estimated to be negligible.

H. Sensitivity to $\Delta G(x)$

Figure 8 shows the calculated asymmetry $A_{c\bar{c}}$ based on five models of $\Delta G(x)$ as a function of p_T, for three momentum ranges of detected single muons, for a photon beam with an endpoint energy of 48.5 GeV. The error bars show the statistical error expected from running 60 full-efficiency hours with the coherent photon beam, plus 18 hours of running with a

target-to-absorber distance increased by $\sim$ 20 cm to measure the rate and asymmetry of muons from pion and kaon decays, and 18 hours running with a 0.2% amorphous radiator (three times thicker than the diamond crystal) to measure the contributions from incoherent bremsstrahlung below 42 GeV. This leads to the relation

$$\delta A_{cc} = \frac{1}{P_b P_t f} \frac{\sqrt{N_{c\bar{c}} + 2N_I + 2N_D}}{N_{c\bar{c}}} \tag{9}$$

where we have used a beam polarization of $P_b = 0.83$, target polarization $P_t = 0.7$, and target dilution factor $f = 0.4$. The number of counts using the coherent diamond beam and the normal close-in absorber position has been broken up into: the components from charm above 42 GeV (denoted by $N_{c\bar{c}}$); counts from all processes below 42 GeV (denoted by N_I); and counts from decay backgrounds (denoted by N_D). Since $2(N_I + N_D)/N_{cc}$ is between 4 and 9 (compare Fig. 5a and Fig. 5c), the statistical errors are on average 2 to 3 times larger than with a purely monochromatic photon beam and no backgrounds.

For the systematic error, we assume an overall relative normalization error of 6% from the combined uncertainties in target and beam polarizations and the target dilution factor. Thus the absolute systematic error on A_{cc} will range between zero and $\sim$ 0.04, depending on how big A_{cc} turns out to be. The systematic error from subtracting the background asymmetries is expected to be small in comparison.

The model asymmetries shown in Fig. 8 were calculated using the Monte-Carlo determined efficiencies as a function of $\hat{s}$ and $|\cos(\theta^*)|$, as illustrated for a few typical bins in Fig. 6. Since only the spin-averaged cross section is used in PYTHIA, we calculated the predicted asymmetries using

$$A_{cc} = \sum_1^N \frac{D(k_i)\Delta\sigma(\hat{s}_i, \cos(\theta_i^*))\Delta G(x_{G_i}, Q_i^2)}{N\sigma(\hat{s}_i, \cos(\theta_i^*))G(x_{G_i}, Q_i^2)}, \tag{10}$$

where N is the number of events with muons in a given kinematic bin. It can be seen that the asymmetries are all negative at low p_T, then change sign at high p_T due to the larger average values of $\hat{s}$. The zero crossing is a basic test of the dominance of the photon-gluon fusion mechanism, while the asymmetry at lower p_T provides the best sensitivity to models of $\Delta G(x)$.

The predictions at $p_T \sim 0.5$ are for the asymmetry to become more negative at high momentum, reflecting the more forward angles selected by higher momentum at fixed p_T. Thus the comparison of data to models versus momentum maps the x dependence of $\Delta G(x)$, while the p_T dependence is a good test of the reaction mechanism. The predicted errors for this proposal are small enough to clearly distinguish models of $\Delta G(x)$ that differ from each other by as little as 10% on average for $x > 0.1$.

A better way to probe the x-dependence of $\Delta G(x)$ is to use lower beam energies (which lowers s and hence raises $\hat{s}/s$. The projected errors for three lower energy ranges are shown in Fig. 9. Again, the projected errors bars are sufficient to clearly distinguish between models. As the photon energy is decreased, the best sensitivity comes from increasingly lower muon momenta, so the results are plotted for 3 to 5 GeV muons at the lowest endpoint energy we expect to use: 19.4 GeV.

We plan to make measurements at a total of 10 electron beam energies between 19.4 and 48.5 GeV, in multiples of 3.24 GeV to keep the polarization longitudinal at the radiator. For each endpoint energy, the diamond crystal angle will be adjusted to keep the bulk of the coherent radiation in the highest 6.6 GeV of the spectrum, so that the average photon energies will be 3.3 GeV less than the endpoint energy. A comparison of the projected statistical errors with different asymmetry models is shown in Fig. 10 for muons with $3 < P < 10$ and $0.5 < P_T < 0.8$ as a function of the average photon energy. This plot illustrates the strong statistical power of this experiment to measure both the shape and magnitude of ΔG. The shape of A_{cc} will be very well determined, since most of the experimental systematic errors are independent of energy (such as target polarization, beam polarization, and dilution factor). Many theoretical errors will depend only very weakly on beam energy, such as the scale at which ΔG is evaluated.

I. Comparison with other Open Charm proposals

The COMPASS experiment [20] expects to obtain an error on a single measurement of A_{cc} of about ± 0.04 at an average photon energy of about 55 GeV. This is about seven times larger than our projected statistical error of ± 0.006 at 45 GeV. The proposed charm upgrade to the HERMES experiment at DESY [21] quotes an error of ± 0.45 on A_{cc} at an average photon energy of about 25 GeV, to be compared with our projected statistical error of ± 0.01 at this photon energy. The HERMES proposal also plans to measure the asymmetry in J/ψ photoproduction. If protons are eventually polarized at HERA and collided with polarized electrons, the authors of [22] predict an error of ± 0.03 on A_{cc} for the x range of the present proposal ($0.1 < x < 0.5$). While the sensitivity at $x > 0.1$ is an order of magnitude worse than for our proposal, HERA can also probe much lower x regions, down to 0.01, with errors that are typically an order of magnitude smaller than the models, so that polarized HERA results would be complementary to the SLAC results in making a precise determination of $\Delta G(x)$ over a large range of $0.01 < x < 0.5$.

J. Comparison to RHIC

An experiment planned at RHIC aims to look at polarized gluons using the reaction $q + g \rightarrow q + \gamma$, tagged by a high p_T photon. Backgrounds arise from π^0 decays and direct photons from $q\bar{q}$ interactions. The projected sensitivity to $\Delta G(x)/G(x)$ is about 0.01 to 0.3 from $0.05 < x < 0.3$. In the region of overlap ($x > 0.1$), this is approximately ten times larger than the statistical errors of the present proposal. Since a completely different reaction is used, the comparison with open charm results will provide a valuable check on systematic corrections to both methods.

K. Gluon Polarization from J/ψ events

The spectrometer described below will have very good acceptance for detecting J/ψ particles that decay to two muons. In the color singlet model [18], inelastic J/ψ's with $z < 0.9$ and $p_T > 0.5$ are dominantly produced by photon gluon fusion. If contributions from color octet production and other higher order diagrams can be understood theoretically, the reaction can also be used to measure ΔG. The cross section for inelastic J/ψ is about 20 times smaller than for open charm, while our detection efficiency is about 3 times better, so we estimate that we will be able to measure the J/ψ asymmetry with approximately three times larger errors than for open charm. The coherent bremsstrahlung beam has a great advantage here over using the bremsstrahlung difference method, since with coherent radiation it is much easier to separate elastic from inelastic J/ψ events. We will also measure the asymmetry for elastic J/ψ with errors about 3 times as large as for open charm. There has been speculation that elastic J/ψ production may be sensitive to $\Delta G(x)$ squared, rather than the linear dependence on $\Delta G(x)$ for open charm, but this question needs further theoretical study.

III. EXPERIMENTAL APPARATUS

A. Polarized Photon Beam

Fig. 11 shows an overall layout of the photon beam. It is very similar to the setup used previously in 1973 in SLAC experiment E78 [33] to produce a quasi-monochromatic photon beam by collimation of coherent and incoherent bremsstrahlung from a thin diamond radiator.

The polarized photon beam is produced using bremsstrahlung from 19.4 to 48.5 GeV polarized electron beams transported through the SLAC A-line. The beam energies will be multiples of 3.237 GeV to preserve longitudinal polarization (with small adjustments at high energy to account for synchrotron radiation). We assume an electron beam with

characteristics similar to those obtained for E154: an intensity of 1×10^{11} electrons per pulse; repetition rate of 120 Hz; pulse length of 250 nsec; and polarization of about 83%.

For most of the running, the electrons will be incident on an existing 0.0007 radiation length (r.l.) thick oriented diamond crystal with a tilt angle θ_0 of a few milliradians. The diamond will be positioned using the SLAC goniometer [34], presently preserved in Beam Line 19 at SLAC. The goniometer can hold two radiators, and position either of them at well-defined angles with respect to the beam axis, in steps of 25 μrad. The goniometer should be usable in it's present state, although the computer interface to the stepping motors has to be modernized, and the entire assembly installed at the end of the A-line. The goniometer will be located just downstream of the Q27/Q28 quad pair at the end of the A-line, as in SLAC E78 [33].

We would like to have the two existing thicker diamond crystals thinned down to the same thickness as the thin crystal (0.07% r.l.), to be used as spares. Based on previous experience, it probably will be necessary to change crystals once or twice during the experiment, due to radiation damage to the lattice.

The electron beam will be about 10 mm wide and 2 mm tall at this location at 48.5 GeV, with the large width due to increased energy spread from synchrotron radiation in the A-line. This is wider than the crystal (8 mm wide), but since the crystal is only held on the bottom, the wider beam will not impinge on unwanted material. At lower energies, the emittance growth due to synchrotron radiation is reduced by approximately the fourth power of the energy, so at 30 GeV the width of the beam will be decreased to a few mm, well contained within the crystal size. Some modest improvements in the A-line optical corrections may be needed to achieve the desired vertical spot size.

The electrons will be bent into a dump using the existing B33-36 dipole magnets, which will need to be refurbished for this experiment. Just upstream of B33, we plan to place a weak magnet with a total field strength of 1 kG-m. This bends 48.5 GeV electrons by 2 mr. The purpose of the initial soft bend is to minimize the number of energetic synchrotron radiation photons impinging upon the polarized target. The B33-B36 dipoles are not strong

enough to bend electrons with $E > 25$ GeV into the existing high power dump. Therefore we will move the magnets to accommodate a smaller bend angle, and use a smaller 100 kW dump for the electrons, positioned downstream of and below the Q38 quadrupole. This will require modifying the vacuum chambers of the magnets.

After entering the End Station, the photon beam passes through a 70 r.l. tungsten collimator, with a diameter of 2 mm, to limit the transverse position and angle of the photons. The electron beam optics will be set to produce maximum photon transmission through the collimator. About 50% to 95% of the photons will hit the collimator (the percentage decreasing with increasing energy due to the smaller m_e/E characteristic bremsstrahlung angle), corresponding to a maximum power into the collimator of 40 Watts for the 0.0007 r.l. diamond radiator, or 100 W for the 0.0020 r.l. amorphous radiator. A rotatable, four-quadrant, tungsten pin-cushion shower-emission detector as used in E78 [35] will be placed just in front of the collimator, and the beam will be centered by matching the signals in the left/right and up/down pairs. Following the collimator are three 18D72 magnets (or equivalent) with a total bending power of 12 T-m. The purpose of these magnets is to sweep away any electrons, hadrons, or muons produced in the collimator. The gaps of the magnets will be reduced with iron to approximately 5 cm to save power; the remainder of the gaps will be filled with lead, except for a 1 cm diameter hole for the photon beam to pass through. The combination of the bending power of the magnets and the energy loss in the lead is enough to divert all Bethe-Heitler muons to a radius larger than that of the spectrometer, so it will not see any of the muons created in the collimator.

The photon beam, after passing through the target and muon spectrometers, will be finally stopped in a Secondary Emission Quantameter (SEQ), used to measure the total photon beam intensity (intensity is energy-weighted flux). Just upstream of the SEQ we will use two auxiliary detectors to monitor the beam flux: an ionization chamber and an atmospheric gas Čerenkov detector. The forward-angle muon spectrometer (see below) will prevent charged particles produced in the target from hitting the three photon beam detectors.

As in E78, the goniometer angles will be calibrated by mapping out the ratio of flux (number of photons) compared to intensity (energy-weighted flux) as a function of horizontal and vertical angles. Maxima in the ion chamber to SEQ ratios occur at well-defined settings, and can be used to determine the correct orientation of the crystal for the desired experimental settings [36].

B. Photon Beam Flux and Polarization

We have calculated the photon beam flux and intensity profile using the formulas given in Eq. 35 of Ref. [37]. We use a constant value of $\psi_1^c = \psi_2^c = 14.0$ for the incoherent contribution, and the values of χ_1^0 and χ_2^0 given in Fig. 10 of Ref. [37] to obtain the coherent contributions. This corresponds to a crystal orientation of $\alpha = \pi/2$, chosen to give the highest possible ratio of coherent to incoherent flux, in contrast to most other experiments which want to maximize linear polarization. We choose the angle θ_0 such that the discontinuity (spike) of the lowest energy coherent peak is always 3.3 GeV below the electron energy. With no collimation, there is a long tail extending to lower energies. This tail is removed by the collimator, as originally proposed in Ref. [38]. The incoherent tail is also reduced by collimation, but in this case the reduction is independent of photon energy. A simple Monte Carlo program was used to fold in the effects of multiple scattering in the radiator, beam emittance, and beam spot size as a function of energy. The resulting intensity spectra for four of the proposed endpoint energies are shown in Fig. 12. The normalization is such that un-collimated incoherent radiation would give an intensity of 14. It can be seen that as the beam energy increases, the incoherent low energy part of the spectrum increases since the collimation angle remains fixed, while the characteristic bremsstrahlung angles decrease as m_e/E. The ratio r of coherent to incoherent photon flux in the upper 6.6 GeV of each spectrum is given at the top of each plot, and is approximately independent of energy, with values ranging from 4 to 6. This is because although coherent radiation at fixed k/E increases linearly with energy, we have kept $E - k_0$ fixed at 3.3 GeV for the lowest energy

spike, and coherent intensity drops approximately linearly with k_0/E at fixed energy. Given the approximately 10% momentum resolution of the spectrometer, the spiky structure of the coherent radiation will play no role in the spectrum of muons from charm decay.

The circular polarization of bremsstrahlung from crystals has been calculated in Ref. [39], and in the reasonable approximation that the two ψ_2 terms are equal to the corresponding coherent and incoherent ψ_1 terms, is simply given by

$$P_\gamma = P_e \frac{1-(1-y)^2-\frac{2}{3}y(1-y)}{1+(1-y)^2-\frac{2}{3}(1-y)} = P_e \frac{y(4-y)}{4-4y+3y^2}.$$

In this approximation, the polarization is the same for the coherent and incoherent components. The results of the full calculation (no approximations) are shown in Fig. 13 for the four spectra of Fig. 12, and are almost indistinguishable from the formula given above, except for some small wiggles near the intensity spikes. It can be seen that the average circular polarization in the upper 6 GeV of the photon spectrum is about 98% of the electron polarization. Averaging over electron spin directions also results in a linear polarization component of the coherent spikes, which will cancel when taking the difference in cross sections for the two electron spin directions. The linear polarization is small due to our choice of crystal orientation and the large values of k_0/E used.

We will measure the product of photon and target polarization as a function of energy using muon pairs with invariant mass between 1.2 and 2.8 GeV (where there are no particle decays) and with net $p_T^2 < 0.2$ GeV^2. With these cuts, the rate is completely dominated by Bethe-Heitler pair production, whose asymmetry can be calculated in terms of the g_1 and g_2 structure functions. For most BH events, the sum of muon energies is the same as the photon energy. The pairs will be measured using both the main muon spectrometer and the small-angle muon detector (see below).

We plan to use Møller scattering to measure the electron beam polarization directly, as in previous E.S.A. experiments. For practical reasons, it will probably be necessary to move the E155 Møller magnet (which has a septum to prevent bending the primary electron beam) and single-arm detectors to a location just downstream of the goniometer.

C. Polarized Target

The target is a 10 cm long, 1 cm diameter cylinder filled with ^{6}LiD (or $^{15}NH_3$), which is polarized using the technique of Dynamic Nuclear Polarization (DNP). Using a dilution refrigerator, in conjunction with a magnetic field of up to 7 T, it is expected that the previous results of 70% polarization [41] for the deuteron and ^{6}Li will be matched.

1. Target Material

Various studies have shown that, to a good approximation, ^{6}Li acts as a polarized proton and a polarized neutron plus an unpolarized spectator α-particle [42]. This results in a spin dilution factor of $f \approx 0.5$ (compared to 0.22 for ND_3), where f is the fraction of polarizable nucleons in the target. Even after taking into account target windows and liquid helium, $f \approx 0.4$, and in conjunction with its high polarization, ^{6}LiD gives a much higher nucleon average polarization than any other solid target. In order to test the hypothesis that protons and neutrons have the same polarized gluon density, we will also use an $^{15}NH_3$ target at the highest beam energy of 48.5 GeV (proton polarization about 90%, $f \sim 0.16$).

^{6}LiD must be pre-irradiated to create the paramagnetic centers necessary for DNP. Abragam and colleagues at Saclay [41,43] were the first to polarize it and obtained 70% for ^{6}Li at a magnetic field of 6.5 T and a temperature of ~300 mK (see Fig. 14). Lower polarizations were obtained at lower fields (64% at 4.9 T; 40% at 2.5 T). The polarizing times are long (~ 20 to 40 hours), but 70% of the final polarization can be obtained in about 10 hours. Further studies at Saclay [44] and investigations at Bonn [45] and PSI [46] have confirmed the ability to reach high polarizations after a few hours of polarizing.

The radiation induced paramagnetic centers are created by irradiating at 185 K, rather than at liquid Argon temperatures (~ 90 K) as is the case with ammonia. At the present time the U. of Virginia polarized target group is studying the polarization properties of ^{6}LiD, as a function of irradiation dose, in preparation for experiment E155. The numerous

irradiation runs for this study are being carried out at the 30 MeV electron Linac on the Stanford University campus in cooperation with Prof. H. Wiedemann and his group. We will gain extensive experience on the in-beam performance of ^{6}LiD during the E155 experiment.

2. Magnet and Microwaves

The polarizing magnet will be a superconducting solenoid operating up to a field of 7 T. Design studies by Oxford Instruments have shown that one of their standard, made-to-order magnets can provide a uniform field region of 5 parts in 10^5 over a volume larger than that of the target cylinder (1 by 10 cm). The magnet has a warm bore of 15 cm diameter and 100 cm overall length. This provides an acceptance for detecting particles out to 0.15 radians without hitting the superconducting coils. Muons at larger angles will traverse the coils after passing through 25 to 50 cm of copper absorber which will be placed in the bore (see below).

Higher field values would require a reduction in the bore diameter or the use of the more expensive Niobium-Tin superconductor if the uniformity specification is to be maintained. In any case the upper limit on the field is defined by the availability of very high frequency microwave tubes with sufficient power for efficient DNP. At the present time, EIO tubes $\sim$ 210 GHz (7.5 T) have been built with $\sim$ 2 watts output. However it is not clear that the potential gain in polarization from the 70% measured at 6.5 T (182 GHz) is enough to justify the extra costs and complexity. Therefore operation will be at about 6.8 T and 190 GHz, which leaves a 7% safety margin on the maximum field of the magnet.

While the bulk of the running time will be on LiD, we plan to run for several weeks at the 48.5 GeV endpoint energy using NH_3. For this target we will run at a magnetic field of 5 T and a temperature of 1 K. These are well-understood conditions in which proton polarizations of greater than 90% are routinely achieved. Operationally, it is quicker to achieve good polarizing conditions than at the lower temperatures used for LiD, because no ^{3}He is involved.

The tuning of the NMR to detect protons at 213 MHz will require no modifications to the Q-meter detectors, as might be the case at 290 MHz (needed at 6.8 T). This can be investigated in the test set-up at UVA. We note that the deuteron NMR frequency at 6.8 T is about 43.5 MHz, well within the Q-meter operational range.

Only external changes to the microwave hardware should be necessary to switch from LiD to NH_3: a 140 GHz tube and associated hardware will replace that for 182 GHz. The EIO power supply will remain the same.

8. Refrigerator

The requirement is for a high power dilution refrigerator with at least 100 mW of cooling power at 300 mK. There is no requirement for operating in the frozen spin mode. The U. of Virginia polarized target group has recently obtained such a refrigerator from CERN. This dilution refrigerator was operated as a target material test facility and was described by Niinikoski and Rieubland [47]. The important features of this refrigerator are: rapid cold access to the mixing chamber for target material changes; fast evacuation and cool down; horizontal operation allowing the beam to go down the axis with minimal material in the way. Figure 15 shows the cooling power performance of this refrigerator. There is potential for improvement as it was originally designed for a circulation rate of 100 mmole/sec but was only operated at up to 60 mmole/sec. However at one point the mixing chamber was modified for another application, so it will have to be unmodified and redesigned to accommodate the size of the target holder. But as described in Ref. [47] it is well matched for DNP of ^{6}LiD.

A large fraction of the heat input to the mixing chamber comes from the microwaves (100 to 200 mW) while the beam contributes no more than about 10 mW.

In summary, the polarized target will primarily use irradiated ^{6}LiD in a dilution refrigerator operating at 300 mK - 400 mK, together with a superconducting warm-bore solenoid at 6.5 T - 7.0 T. For some of the time, NH_3 will be used at a higher temperature and lower

magnetic field.

D. Absorber

It is essential to have an absorber as close to the target as possible to reduce the flux of muons coming from pion and kaon decays. Assuming a minimum diameter of 1 cm for the photon beam to travel from the target to the quantameter, the minimum distance to the absorber is given by $[5 + 0.5/\sin(\theta)]$ cm, or typically 10 cm. The ideal absorber material should have an absorption length comparable to 10 cm, a total of at least eight absorption lengths to completely remove the hadron flux (which is three orders of magnitude larger than the muon flux), and at least 30 radiation lengths to stop the large photon flux (also three orders of magnitude larger than the prompt muon flux). More radiation lengths are not desirable because this degrades the angular resolution through multiple scattering. A further criteria is to have at least 1.2 GeV energy loss to reduce the flux of low energy decay muons hitting the front detectors. The best compromise material seems to be copper, which has a density of 8.96 gm/cm^2, a radiation length of 1.44 cm, and absorption length of 14.8 cm, and an energy loss of 1.45 (1.7) GeV per meter for 2 GeV (10 GeV) muons. Studies with GEANT and the experience of other experiments (such as the Drell-Yan experiments at Fermilab) have shown that placing low Z materials such as graphite and boron after the copper is useful in reducing the neutron flux from hadronic showers.

The absorber arrangement is shown in Fig. 16. Muons emitted between 40 and 100 mrad pass through an average of 90 cm of copper before entering the first detector plane. This will be highly segmented to handle the hadron shower residues. Particles emitted between 5 and 40 mrad pass through 10 to 80 cm of copper, but will not hit the first detector, which starts 3.5 cm from the beam axis. Following the first detector is another 50 cm of absorber. The inner 4 cm radius of this is copper, to continue the absorption of muons emitted between 20 and 40 mrad, before they hit the second layer of detectors. The outer part of this absorber is made from a boron/carbon mixture to absorb the remaining hadronic shower neutrons

and low energy muons produced by hadrons emitted at angles larger than 40 mrad. The inner 1 cm diameter of both the front and rear absorbers will be a vacuum pipe.

In order to measure the asymmetry and rates for decay muons, the front absorber has a 20 cm section in front of the front detectors which can be removed, allowing the front 70 cm of copper to be moved 20 cm downstream.

E. Main Spectrometer

The task of the main spectrometer is to measure the angle, sign, and momentum of muons with $3 < P < 15$ GeV and $20 < \theta < 200$ mrad. This kinematic region is chosen to optimize the ability to distinguish single muons resulting from open charm decays (with $p_T > 0.5$ GeV), from backgrounds with two opposite sign muons (principally Bethe-Heitler production).

A spectrometer design that meets these goals is shown in Fig. 17. A large cylinder of magnetized iron, 2 m in diameter and approximately 3 m long (vertical direction in the lab), is used to provide a fairly uniform solenoidal field of about 2 Tesla at low cost. The field is in the vertical direction (out of the plane of Fig. 17), so particles bend to the left or right. The iron is magnetized by a simple set of relatively low power coils wound around the top and bottom of the cylinder. Each coil carries approximately 70 kA of current, based on our modeling using the two-dimensional POISSON code. The field uniformity is better than 5% in the region 80 cm above and 80 cm below the beam pipe. Approximately 2 m wide, 4 m long, and 50 cm thick iron plates placed above and below the cylinder connect to 2 m by 2 m by 80 cm iron side plates to provide the flux return path. The design is very similar to the SLAC streamer chamber magnet presently located near E.S.A., except that the air gap is filled with iron, the number of ampere-turns needed in the coils is reduced by a large amount, and the overall size is smaller since no camera is involved.

A tapered hole will be cut along the beam axis with an angle of 20 mrad with respect to the target. The field in the hole will be very small, so that charged particles produced at

less than 20 mrad will pass through the spectrometer undeflected and into the forward-angle spectrometer discussed below.

F. Detectors and Resolution

The goal of the detector system is to find muon tracks in an environment where there are up to 10 muons per 250 nsec beam spill passing through the first layers of detectors. This requires excellent timing resolution. The multiple scattering ($\delta p_T \sim 0.1/P$ per meter of iron) and bending power of the magnets ($\delta p_T \sim 0.5/P$ per meter) suggest that the position resolution need not be better than a few cm. The detectors that best meet these requirements are hodoscopes of plastic scintillators.

The arrangement of scintillators is shown in Figs. 16 and 17. The front plane is 40 cm by 40 cm (with a 4 by 4 cm hole around the beam pipe), and is a good match to the front set of six hodoscope planes (u,v,x,y,x,y) in the existing 2.75 degree spectrometer. These planes have a total of 289 narrow (mostly 0.5" or 0.6" wide) scintillators, each with a small (1/2" or 3/4") PMT that provides very good time resolution. The fine granularity and large redundancy should allow the initial muon positions to be defined with an accuracy of 2 mm (sigma), corresponding to an angular resolution of 2 mr. For muons with $P < 25$ GeV, the resolution will be worse due to multiple scattering in the copper, and can be approximated as 50/P mr. This is equivalent to a p_T resolution of 0.05 GeV, independent of P and θ. There will be some additional degradation at large angles due to the finite target length.

The second plane of detectors covers an area of about 60 by 60 cm, with a 4 cm by 4 cm hole around the beam pipe. This plane will be made up of from existing fingers in the E155 5.5 degree spectrometer (front and part of rear hodoscope planes). These fingers are 3 cm wide, but will be overlapped to give an effective position resolution of 4 mm.

The third and fourth planes are placed after the iron, and are used to measure the position and angles of muons deflected in the magnetic field. The third layer is 150 cm tall to match the angular acceptance of ± 20 mrad in y, where y is the vertical direction in the

lab, and x is the horizontal direction perpendicular to the beam line. The fourth layer will be about 150 cm tall and will not cover as wide an x range. It is designed to obtain better momentum resolution for the high momentum and/or small angle muons that come out the central portion of the spectrometer, by measuring the exit angle as well as position. The third and fourth plane scintillators will mostly be new for this experiment, although about a third of them will be made by joining existing hodoscopes together. We will need to acquire about 300 new PMT's, and 150 scintillator bars. The fingers will be 150 cm tall, with PMTs at each end, and the granularity in the x direction (left/right) will range from 3 cm near the beam pipe to 10 cm at the extremes of the arcs. The y positions will be determined by measuring the time difference between the PMTs at each end of each bar. The fingers will be overlapped, so that a muon will always traverse two bars. The PMTs of the third layer will be about 40 cm above or below the magnet coils, in a region where the magnetic field in the air is low enough that conventional shielding techniques will be adequate to reduce the fields at the tubes to acceptable levels.

The granularity of the bars is matched to the intrinsic momentum resolution for muons traversing 2 m of iron. Since both multiple scattering and bending are proportional to $1/P$, the intrinsic momentum resolution is about 15%, independent of momentum. The deflections of the high momentum particles are smaller than for the low momentum particles, but the high P muons also emerge closer to the beam pipe, so that the fine granularity is only needed in this region. Figure 18 shows a sample of various trajectories through the spectrometer: the large effects of multiple scattering are clearly visible.

The resolution in the invariant mass of a pair of muons will be about 15%, dominated by the momentum resolution of the main spectrometer, which is adequate to differentiate J/ψ decays from Bethe-Heitler events, although it will not be possible to distinguish between muon decays from ρ's and ϕ's, or to see the ψ' peak.

G. Forward Angle Muon Spectrometer

An 18D72 dipole (or equivalent) placed just downstream of the main spectrometer will be used to analyze muons produced in the target at angles less than 20 mr (the smallest angle seen by the main spectrometer). The spectrometer will also sweep out other charged particles (mostly electron pairs) to prevent them impinging upon the ionization chamber and SEQ. A pair of 20 cm by 150 cm scintillator hodoscopes will be placed just in front of the ion detector to measure the momenta of small angle muons. Two meters of iron will be placed in front of these detectors to stop electrons and hadrons. From the sum of the muon momenta for muons in time coincidence, we will get a continuous monitor of the beam flux versus photon energy, for energies between 10 and 48 GeV. The rate of small angle muon pairs will be about 20/spill, and the photon energy resolution will be about 10%.

H. Electronics and Data Acquisition

The electronics consists of a discriminator (LeCroy 4413 or 3412) and a multi-hit TDC (LeCroy 2277 or 3377) for each scintillator PMT. Each PMT may also be read out by a LeCroy 2280 ADC to measure the pulse height integrated over each beam spill. Assuming they all remain available, there are almost enough discriminators, TDC's, fanouts, and TDC's presently in End Station A to carry out the present proposal. The data acquisition system will be similar to that used in E155. The expected data rate is much lower than for E155, so no major upgrades in speed or storage capability will be needed.

IV. REQUEST TO SLAC

We request a total of four calendar months of running at a the full repetition rate of 120 Hz. This assumes that the run takes place between PEP-II fills with an average efficiency of 55%, with a further 25% inefficiency for maintenance days, target repairs, and problems with detectors or data acquisition. This gives a net efficiency of about 40%. If the run occurs

in a dedicated mode (not concurrent with PEP-II), the time needed would be shortened to two months. The running time will be divided approximately equally among beam energies of 19.7 to 48.5 GeV (in steps of 3.24 GeV). At each energy, data will be taken with the diamond radiator for about 75% of the time and with the amorphous radiator for 25% of the time. For each radiator, most of the running time will be with the absorber position close to the target, with the remainder in the position away from the target. The NH_3 target will be run at 48.5 GeV only, while the LiD target will be used at all energies.

We also request one month of checkout running. This can be done at a lower repetition rate (30 to 60 Hz) and a relatively low beam energy of 29.1 GeV. The checkout time will be used to debug the spectrometer detectors, study beam-related backgrounds (and possibly change the shielding and collimation arrangement, if required), and to align and measure the coherent photon beam. We will also measure the various physics backgrounds to optimize the run plan with full beam current.

We request SLAC to provide resources needed to implement the coherent bremsstrahlung apparatus at beam energies up to 48.5 GeV. The collaboration will furnish the beam detectors (ionization, Čerenkov, SEQ, and small angle muon detectors). The collaboration will provide many of the target components, such as the dilution refrigerator, and the manpower for initial tests of the target systems at the University of Virginia and for testing at SLAC. We request that SLAC provide the technical and financial support for the necessary modifications and upgrading of the refrigerator and its associated systems and the on-site assembly and testing to meet the more rigorous requirements of this experiment operating in E.S.A.. This would include major systems such as a 182 GHz microwave assembly, 10 Q-meters for NMR measurement with three coils and a set of sealed Roots pumps with 6000 m^3/hr pumping capacity. In addition we ask that SLAC buy the 7 T solenoid. Members of the collaboration have experience in setting up and operating such magnets, but would need some additional technical support. The existing supply of ^{6}LiD and NH_3 from E155, though adequate for the present proposal, could be supplemented. We will investigate the possibility of obtaining ^{6}LiD which has been depleted of ^{7}Li (the E155 samples have about

5% ^{7}Li), and of operating with rods, rather than chips, of material (both lithium deuteride and ammonia), which will require irradiation.

We request SLAC to provide the magnet for the spectrometer, and to augment the supply of scintillators and PMTs existing in E155 by about 20%. The collaboration will undertake the assembly and testing of the scintillators. We request that the electronics and data acquisition system of E155 be left available for the present proposal, so that at most very modest upgrades will be needed.

V. ACKNOWLEDGMENTS

We thank V. Breton, S. Brodsky, R. Gardner, D. Pierce, E. Quack, T. Sjostrand, R. Vogt, and many others for useful discussions and other assistance.

REFERENCES

[1] SLAC E142, P. L. Anthony *et al.*, Phys. Rev. D 54 (1996) 6620.

[2] SLAC E143, K. Abe *et al.*, Phys. Rev. Lett. 74 (1995), 346.

[3] SLAC E143, K. Abe *et al.*, Phys. Rev. Lett. 75 (1995), 25.

[4] J. D. Bjorken, Phys. Rev. 148 (1966), 1467; Phys. Rev. D 1 (1970), 1376.

[5] EMC, J. Ashman *et al.*, Phys. Lett. B206 (1988), 364; Nucl. Phys. B328 (1989), 1.

[6] J. Ellis and R. Jaffe, Phys. Rev. D 9 (1974), 1444; D 10 (1974), 1669 (E).

[7] G. Altarelli and W. J. Sterling, Particle World 1(2), 40 (1989); G. Altarelli and G. G. Ross, Phys. Lett. B212, 391 (1988).

[8] G. Altarelli and G. Parisi, Nucl. Phys. B126 (1977), 298; V. N. Gribov and L. N. Lipatov, Yad. Fiz. 15 (1972), 781 [Sov. J. Nucl. Phys. **15** (1972), 438].

[9] E. B. Zijlstra and W. L. van Neerven, Nucl. Phys. B417 (1994), 61; R. Mertig and W. L. van Neerven, Z. Phys. C70, 637 (1996) and INLO-PUB-12-95, September 1995.

[10] R. D. Ball, S. Forte, and G. Ridolfi, Phys. Lett. B378 (1996) 255.

[11] M. Glück, E. Reya, M. Stratmann, and W. Vogelsang, Phys. Rev. D 53 (1996) 4775.

[12] S. J. Brodsky, M. Burkardt, and I. Schmidt, Nucl. Phys. B441 (1995), 197.

[13] T. Gehrmann and W. J. Stirling, Phys. Rev. D 53 (1996) 6100.

[14] R. L. Jaffe, Phys. Lett. B365, 359 (1996).

[15] I. I. Balitsky, V. M. Braun and A. V. Kolesnichenko, Phys. Lett. B242 (1990), 245; B318 (1993), 648 (E); X. Ji and P. Unrau, Phys. Lett. B333 (1994), 228; E. Stein, P. Cornicki, L. Mankiewicz, A. Schafer, Phys. Lett. B353 (1995), 107.

[16] D. L. Adams *et al.*, Phys. Lett. B336, 269 (1994).

[17] G. Bunce *et al.*, Particle World 3, 1 (1992).

[18] M. Gluck and E, Reya, Z. Phys. C39, 569 (1988).

[19] J. J. Aubert *et al.*, Nuc. Phys. B213, 31 (1983).

[20] COMPASS proposal, CERN/SPSLC -96-14 (March, 1996).

[21] M Amarian *et al.*,, DESY-PRC97/03 (January, 1997).

[22] S. Frixione and G. Ridolfi, hep-ph/9605209 (May, 1996).

[23] M. Fontannaz, B. Pire, and D. Schiff, Z. Phys. C11, 211 (1981).

[24] J. C. Anjos *et al.*, Phys. Rev. Lett. 65, 2503 (1990).

[25] T. Sjostrand, Computer Physics Commun. 82, 74 (1994).

[26] P. L. Frabetti *et al.*, Phys. Lett. B370, 222 (1996).

[27] K. Abe *et al.*, Phys. Rev. D 33, 1 (1986).

[28] D. Wiser, PhD thesis, University of Wisconsin, 1977 (unpublished).

[29] D. Ritson, SLAC-PUB-1728 (1976), published in Nashville Conf. 1976:75.

[30] F. Sabatie, E154 Technical Note 45 (October 1996).

[31] Y.S. Tsai, Rev. Mod. Phys. 46 (1974) 815; 49 (1977) 421 (E).

[32] R. Yoshida, Nucl. Instrum. Meth. A302 (1991) 63.

[33] W. Kaune et al., Phys. Rev. D 11, 478 (1975).

[34] R. Schwitters, SLAC-TN-70-32 (1970).

[35] G. Miller and D. Walz, SLAC-PUB-1297.

[36] D. Luckey and R. Schwitters, Nucl. Instrum. Meth. 81, 164 (1970).

[37] G. Diambrini Palazzi, Rev. Mod. Phys. 40, 611 (1968).

[38] R. F. Mozley and J. DeWire, Nuevo Cimento 27, 1281 (1983).

[39] I. M. Nadzhafov, Bulletin of the Academay of Sciences of the USSR, Physcal Series Vol 14, No. 10, p. 2248 (1976).

[40] V. M. Kuznetsov and A. P. Potylitsyn, Yad. Fiz. 27 (1977) 149 [Sov. J. Nucl. Phys. 27 (1978), 79].

[41] A. Abragam *et al.*, J. Physique - Letts., 41, L-309 (1980).

[42] N. W. Schellingerhout *et al.*, Phys. Rev. C 48, 2714 (1993).

[43] V. Bouffard *et al.*, J. Physique, 41, 1447 (1980).

[44] G. Durand *et al.*, Proc. Int. Symp. on High Energy Spin Physics, Nagoya, Japan 1992, eds. T. Hasegawa *et al.*, p. 355.

[45] S. Goertz *et al.*, Nucl. Instrum. Meth. in Phys. Res., A356, 20 (1995).

[46] B. van den Brandt et al., Proc. 9th High Energy Spin Physics Symp. Bonn, Germany, 1990, p. 320.

[47] T. Niinikoski and J. Rieubland, Proc. Ninth Cryo. Eng. Conf., Kobe, Japan, 1982, p. 580.

TABLES

decay to	D^+	D^0	D_s^+	Λ_c^+	K^+	π^+	τ^+
μ^+	4400	6000	1000	700	180	80	50
decay to	D^-	$\bar{D}^0$	D_s^-	Λ_c^-	K^-	π^-	τ^-
μ^-	6100	8100	900	100	100	100	30

Table I. Number of detected muons with $p_T > 0.5$ GeV from decays of the parent particles listed, for a sample of open charm events generated using PYTHIA with a photon beam with endpoint energy 48.5 GeV impinging on a deuterium target. The event sample corresponds to four minutes running time at the design luminosity. The parents of the kaons, pions, and τ's are D mesons. The kaon and pion decay distance was limited to 25 cm.

FIGURES

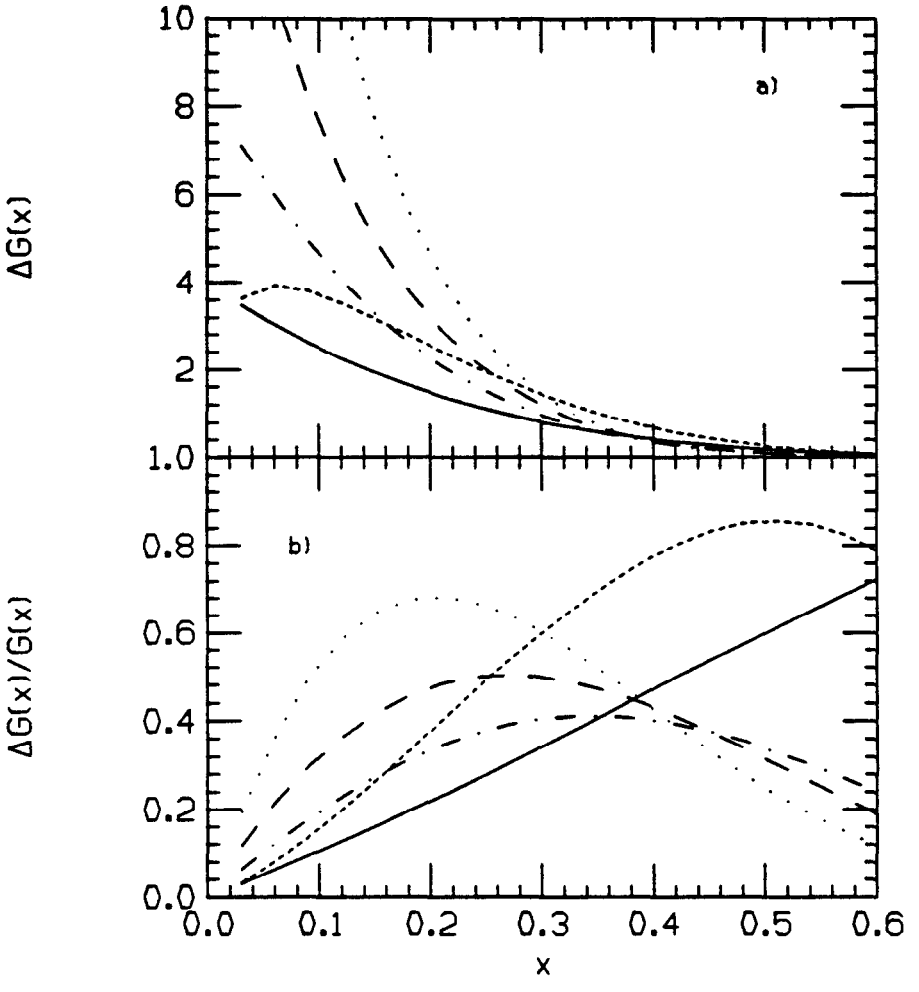

FIG. 1. The polarized gluon density $\Delta G(x)$ for five representative models (see text): a) $\Delta G(x)$; b) $\Delta G(x)/G(x)$.

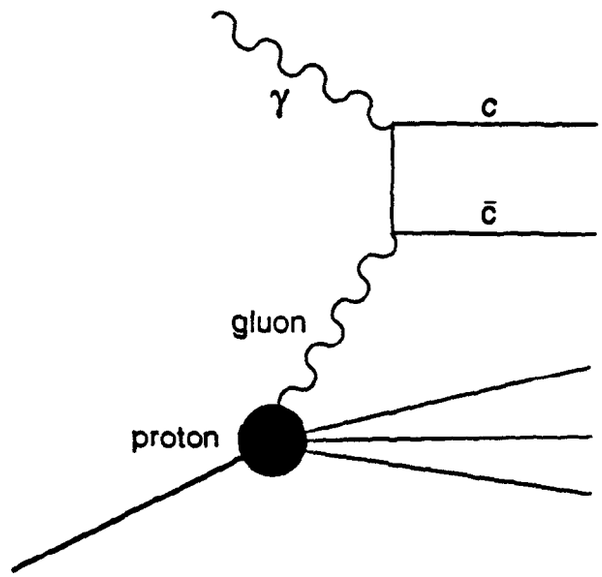

FIG. 2. The photon-gluon fusion diagram.

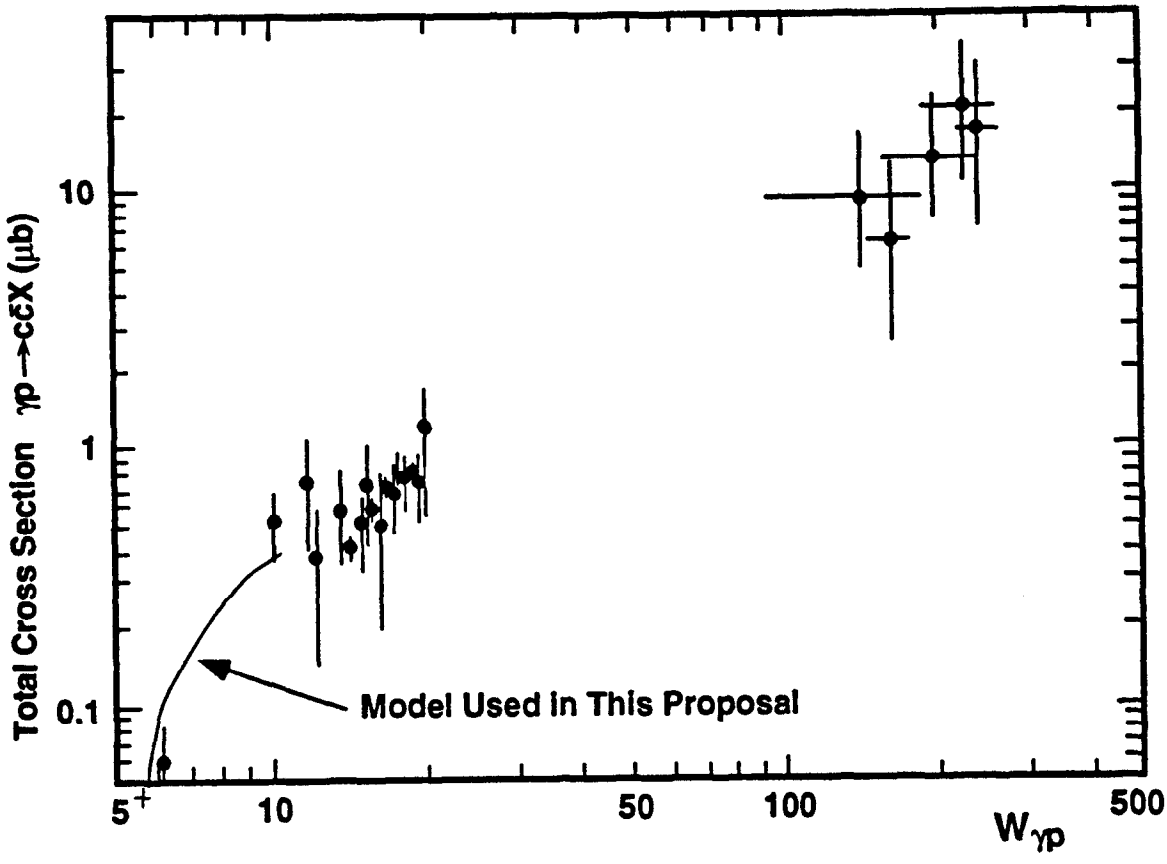

FIG. 3. Compilation of world data on the total open charm photoproduction cross section. The model used for the W range of this proposal (5.2 to 10 GeV, corresponding to photon energies of 16 to 48 GeV), is shown as the solid curve.

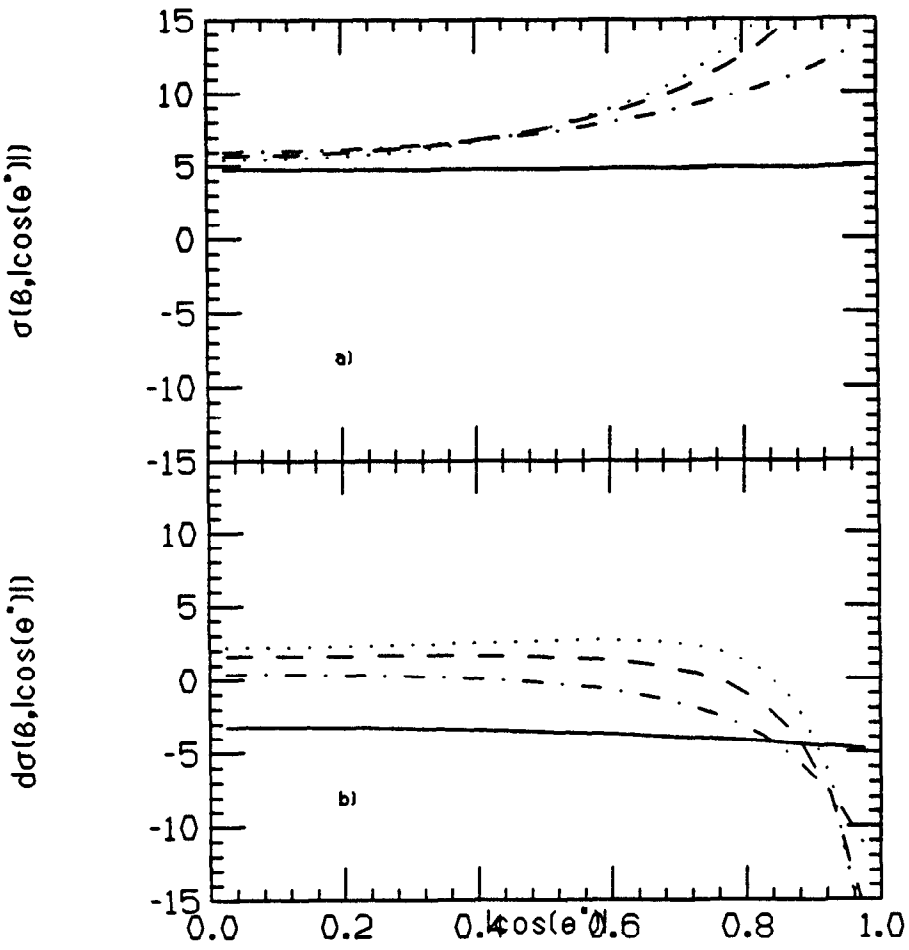

FIG. 4. The a) spin-averaged and b) spin-dependent cross sections for $\gamma g \to c\bar{c}$ (scaled by $9\hat{s}/8\pi\alpha\alpha_s(\hat{s})$, and assuming $m_c = 1.5$ GeV) as a function of $\cos(\theta^*)$ for four values of $\hat{s}$: 10 (solid curve); 20 (dash-dot), 30 (dashes); and 40 GeV^2 (dots). The corresponding values of β are 0.3, 0.74, 0.84, and 0.88.

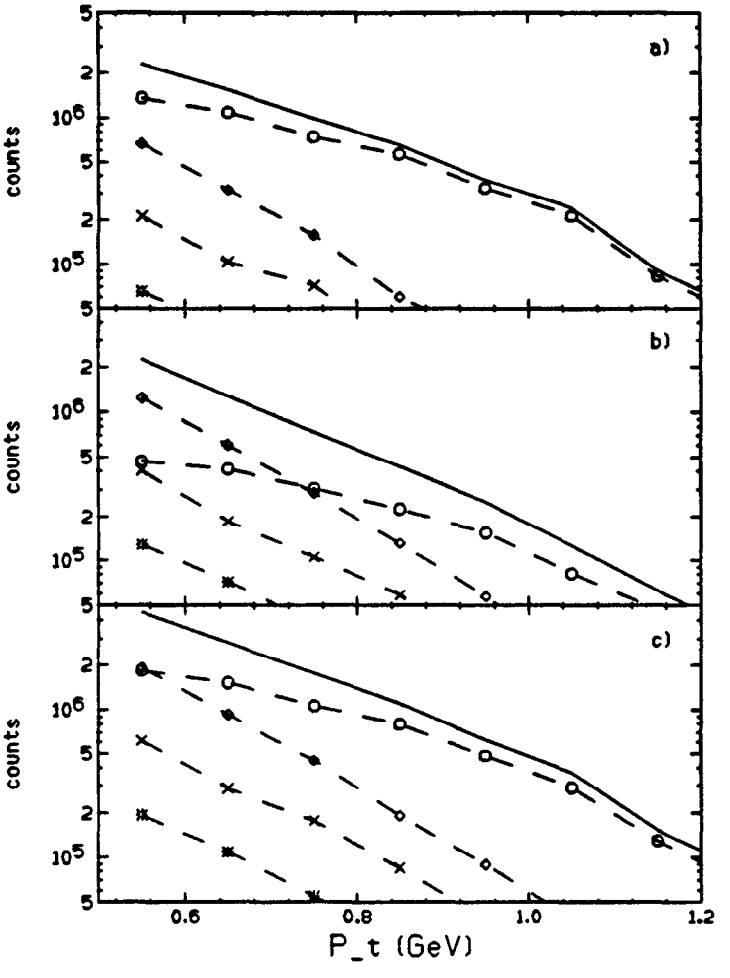

FIG. 5. Number of counts per 0.1 GeV bin in p_T as a function of p_T of single muon events with momenta $5 < P < 10$, for 60 hours of full efficiency running for a diamond crystal photon beam, for a) photons between 42. and 48.5 GeV only; b) photons below 42 GeV; c) all photons. The open charm counts (the experimental signal) are the open circles, the decays from pions and kaons are shown as the diamonds, Bethe-Heitler counts are the crosses, and decays of η, ρ, ω, and ϕ are shown as the stars. The sum of all the counts is shown as the solid curve. Only events with a single detected muon are shown (events with two muons in time coincidence, mostly BH background events, have been eliminated).

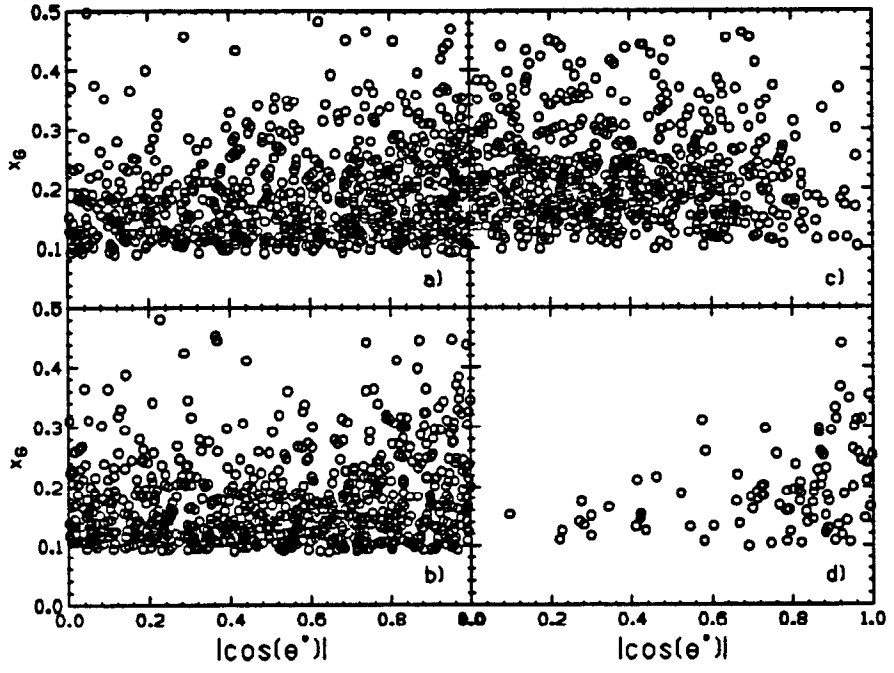

FIG. 6. Distribution in $x = \hat{s}/s$ and $\cos(\theta^*)$ for photon with energy $39 < k < 48.5$ GeV for: a) all $c\bar{c}$ events; b) those leading to a final state muon with $5 < P < 10$ GeV and $0.6 < p_T < 0.7$ GeV; c) those leading to a final state muon with $5 < P < 10$ GeV and $p_T > 1.0$ GeV; d) those leading to a final state muon with $15 < P < 20$ GeV and $0.6 < p_T < 0.7$ GeV.

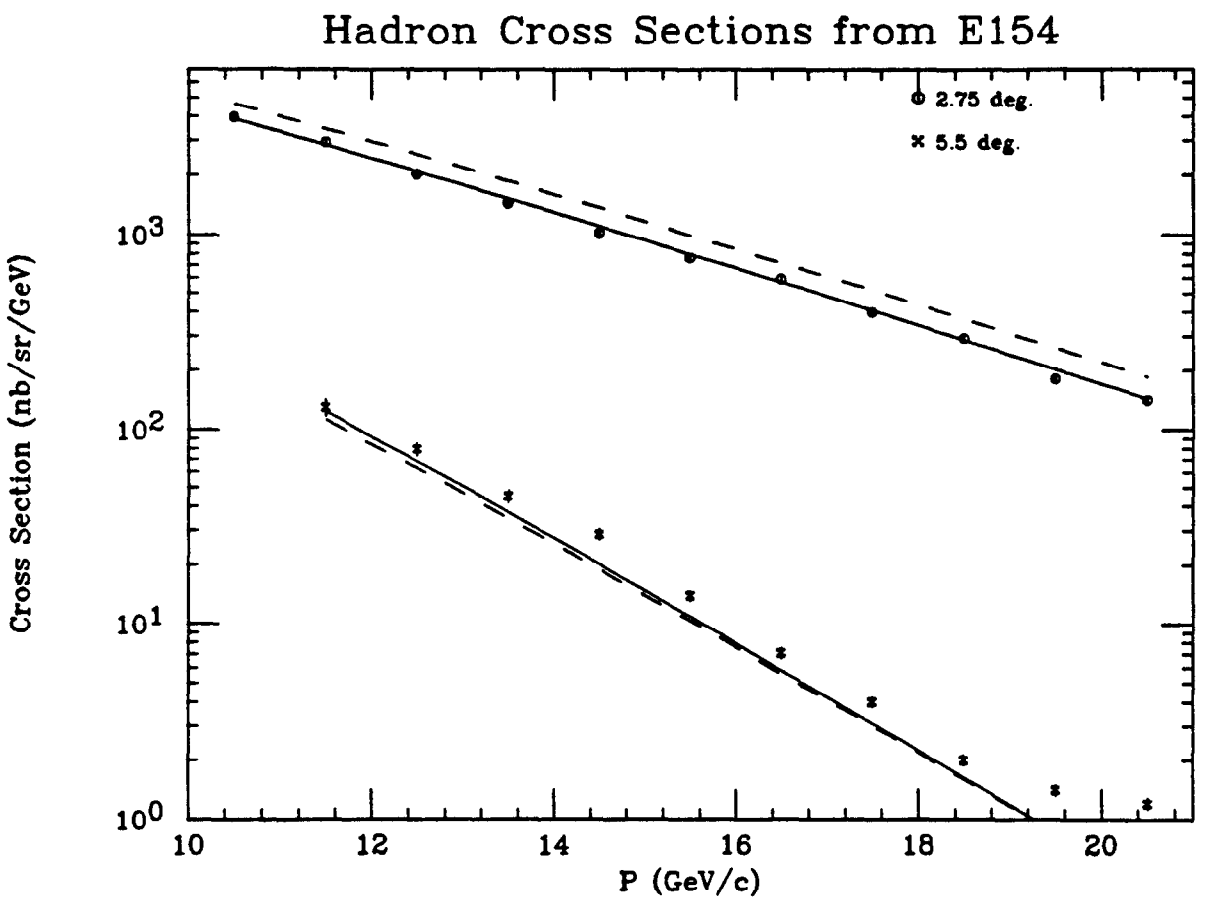

FIG. 7. Inclusive electroproduction cross sections for negative hadrons measured in SLAC E154 from a glass/helium target with a beam energy of 48.5 GeV at 2.75 and 5.5 degrees. The solid lines are the predictions from the Wiser fit, while the dashed lines are from PYTHIA.

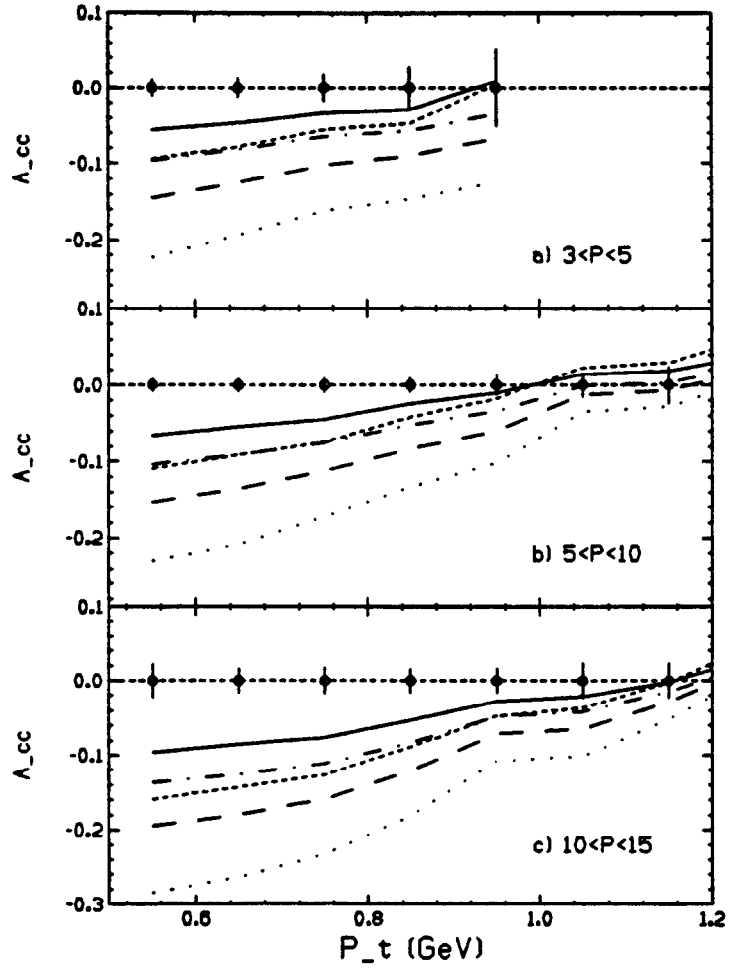

FIG. 8. Theoretical predictions for the open charm asymmetry A_{cc} for the five models of Fig. 1, as a function of muon p_T, for photons between 42 and 48.5 GeV. The data points show the projected statistical error bars for this proposal. Systematic errors will be approximately $0.06A_{cc}$. The muon momentum ranges are: a) 3 to 5 GeV; b) 5 to 10 GeV; c) 10 to 15 GeV.

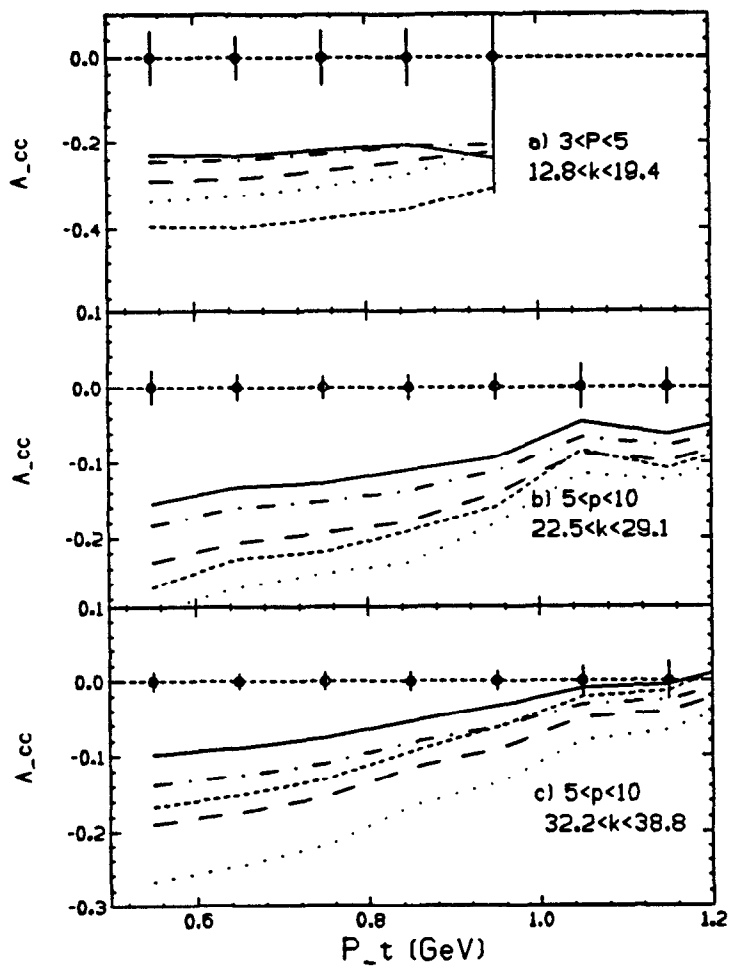

FIG. 9. Same as Fig. 8 but at the lower photon energy ranges shown on the plots. The range of muon momenta are also shown.

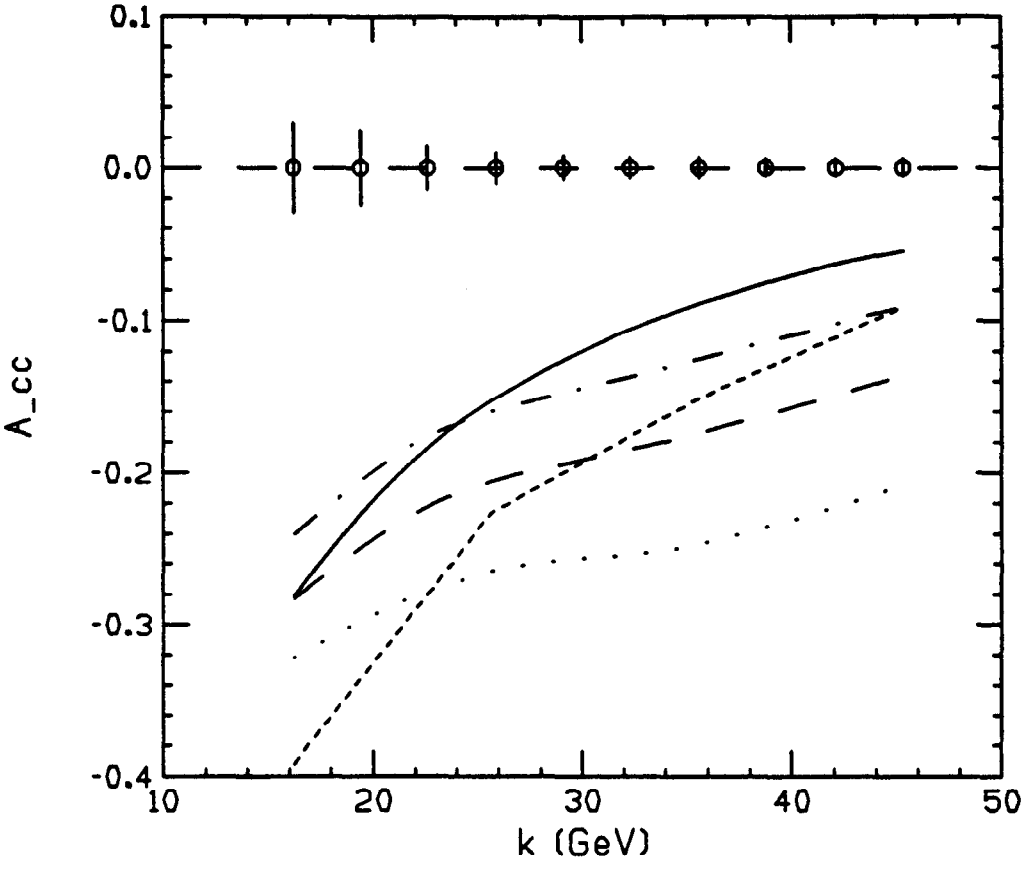

FIG. 10. Asymmetries for the five models of Fig. 1 as a function of average photon energy, with open charm events tagged by single muons with $3 < P < 10$ GeV and $0.5 < P_T < 0.8$. The points indicate the projected statistical errors for the running conditions given in the text. Experimental systematic errors will be highly correlated from point-to-point, and will be approximately 0.06 of the measured asymmetries.

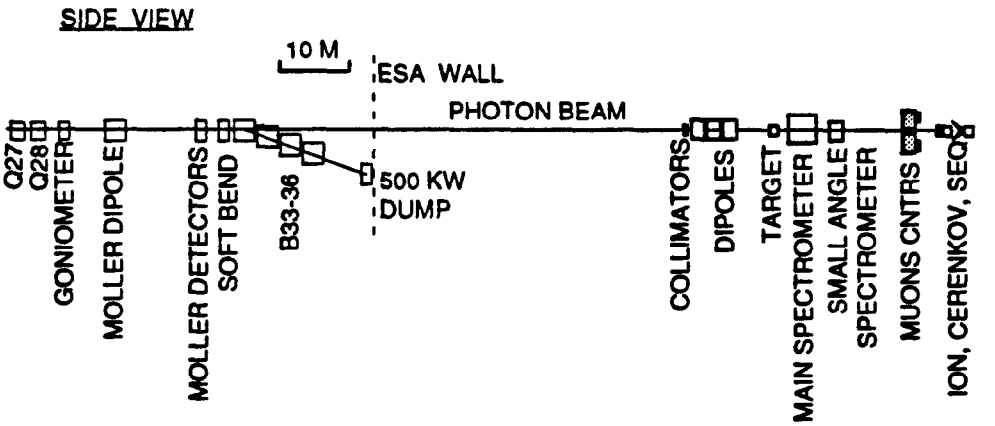

FIG. 11. Overall side view layout of the experiment (scale is approximate).

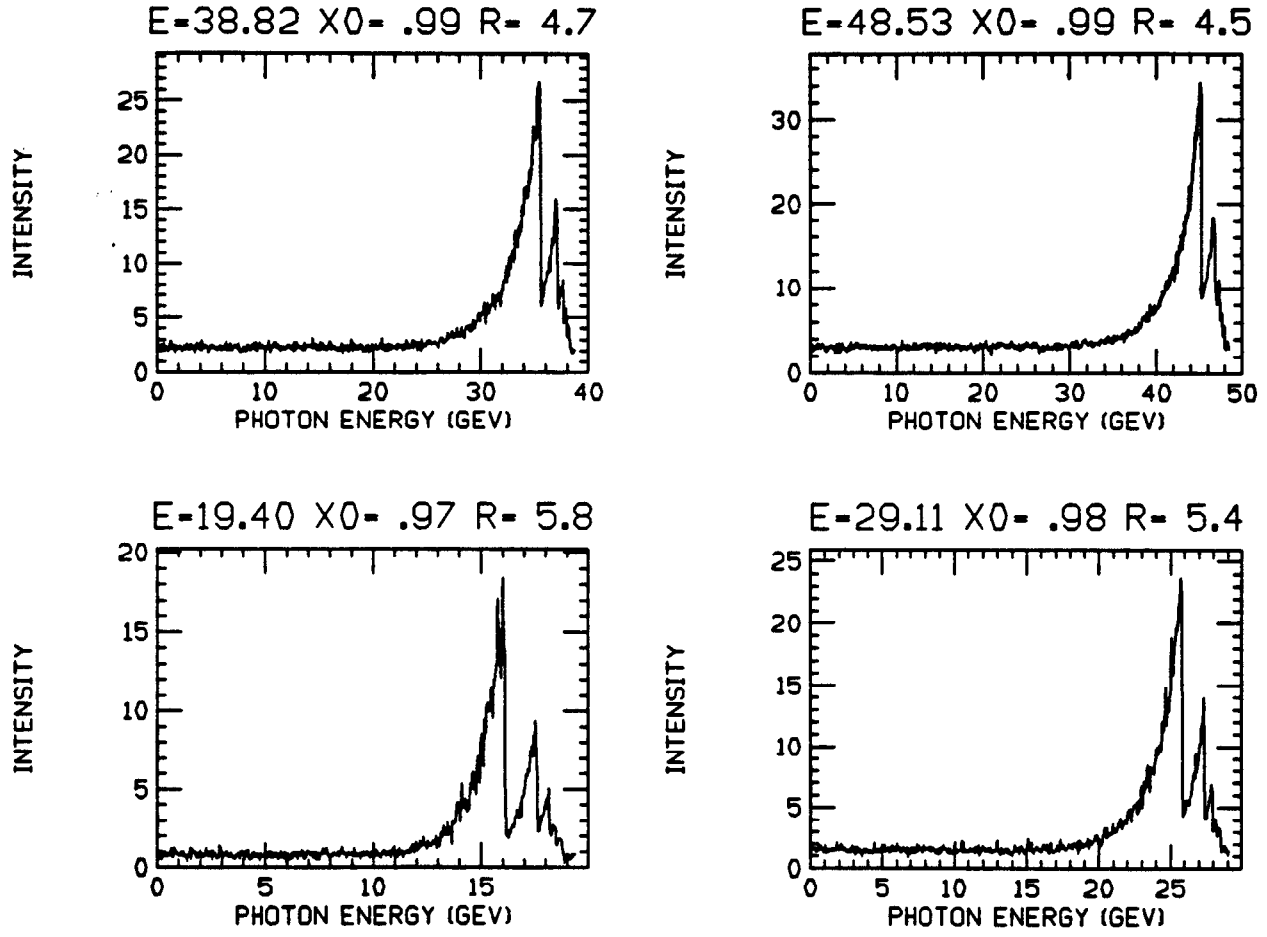

FIG. 12. Intensity spectra of photons from 0.0007 r.l. diamond radiator at the four beam endpoint energies shown. The spikes in the upper 6.6 GeV of each spectrum are from coherent radiation. Effects of collimation, multiple scattering, beam size, and beam emittance have been taken into account. The normalization is such that un-collimated incoherent radiation would give an intensity (energy times flux) of 14.

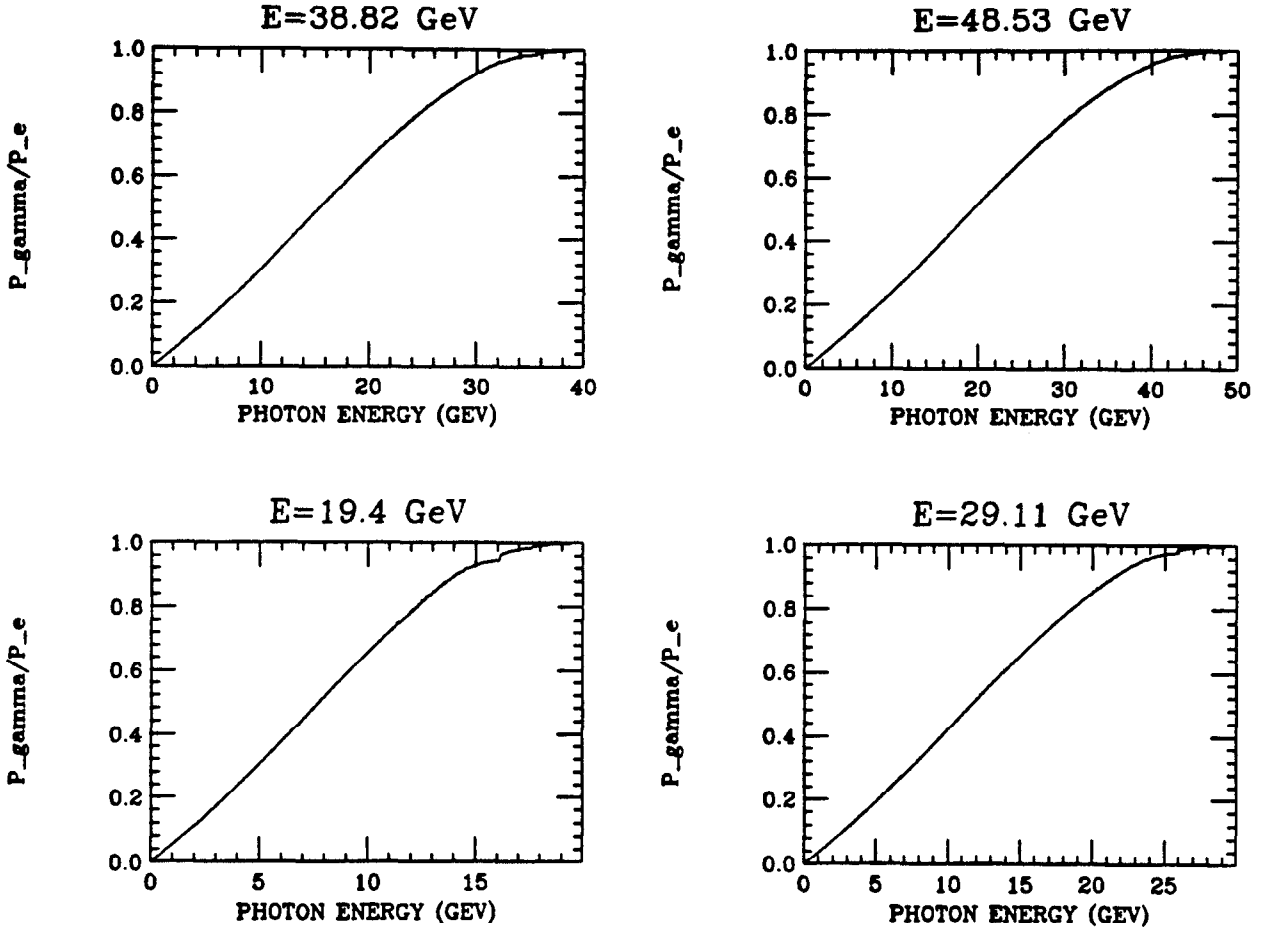

FIG. 13. Relative circular polarization of photons for the spectra of the previous figure. The polarization is relative to that of the electron beam.

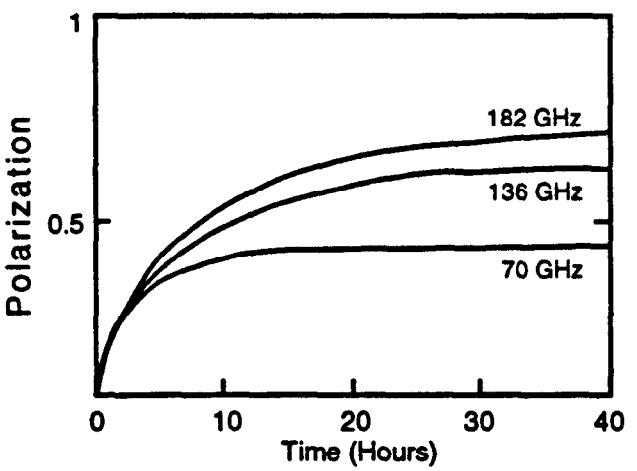

FIG. 14. Polarization of ^{6}Li measured by Abragam et al. as a function of time for three combinations of field and frequency. The upper curve corresponds to the conditions of this proposal.

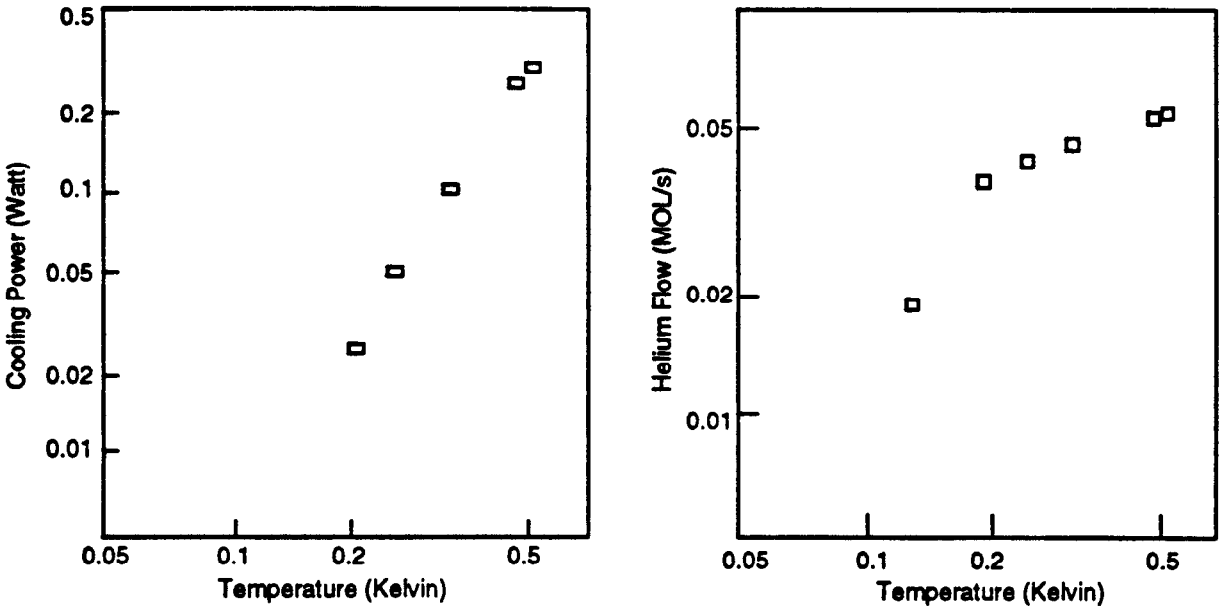

FIG. 15. Cooling power for the refrigerator of this proposal (open squares) as a function of temperature. The relation between temperature and helium flow is also shown.

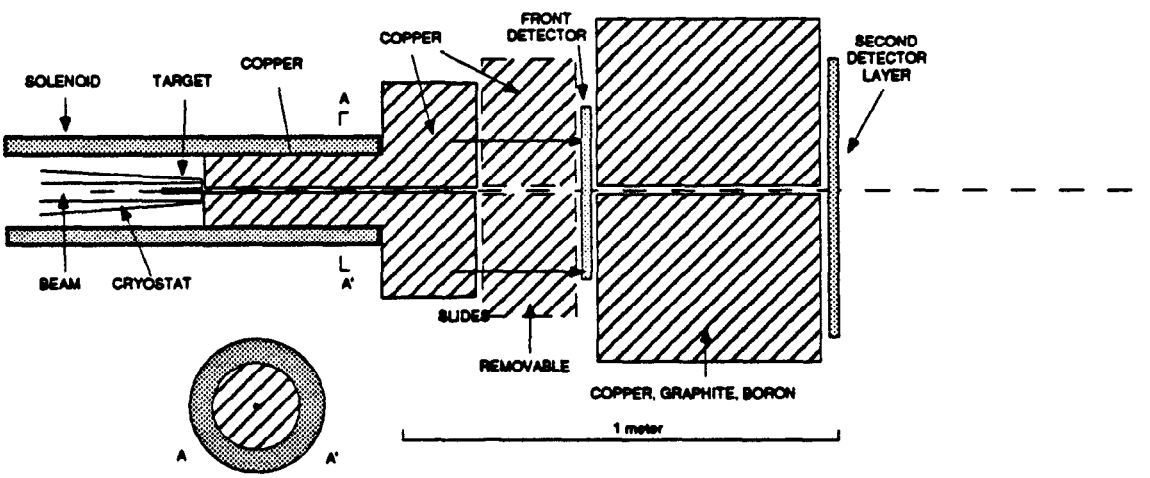

FIG. 16. Layout of the target, absorbers, and front two detector planes. The view is the same from the side or the top.

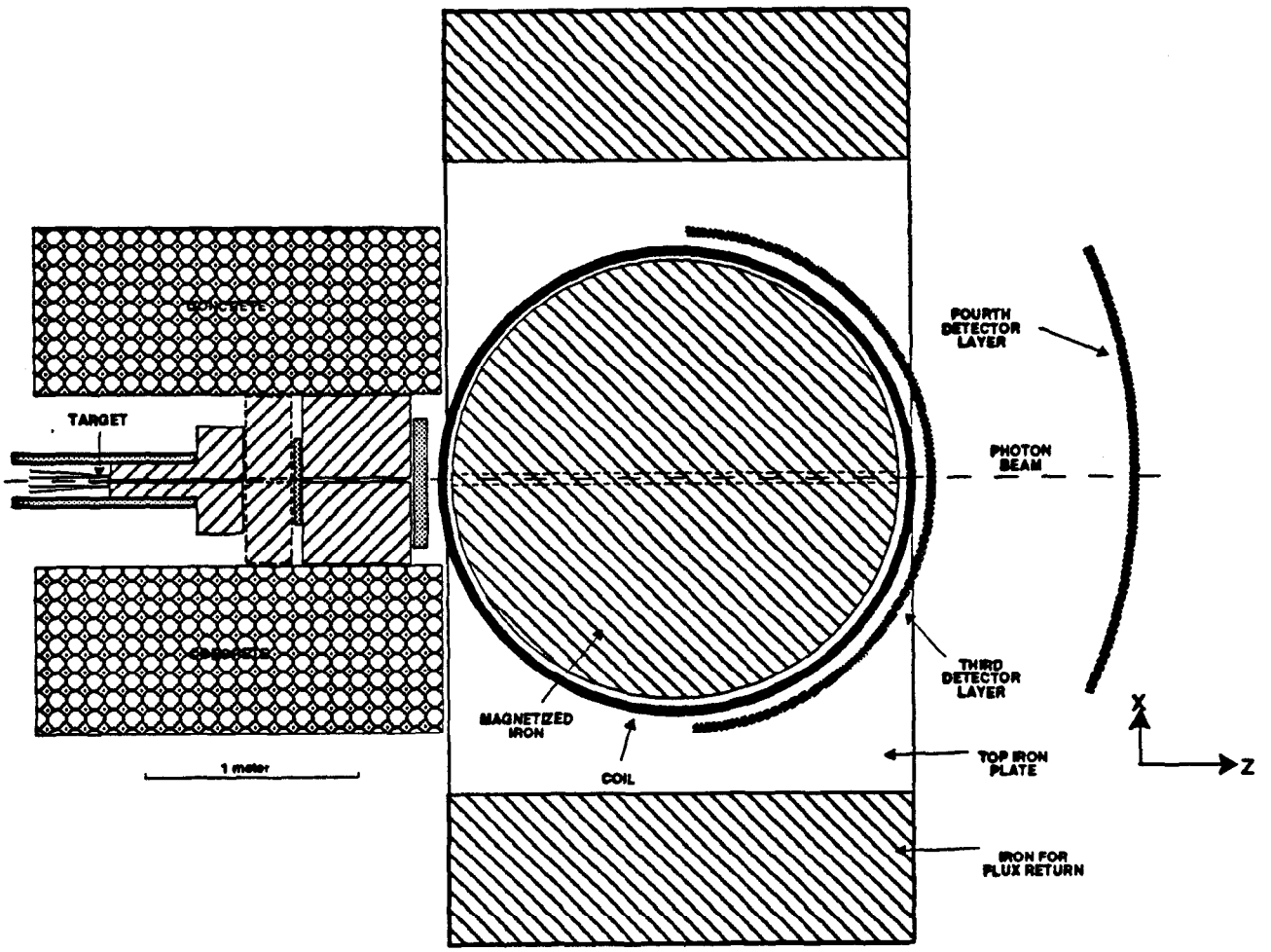

FIG. 17. Layout of the main spectrometer system (top view). The forward angle spectrometer dipole is 1 m down-beam of the fourth detector plane.

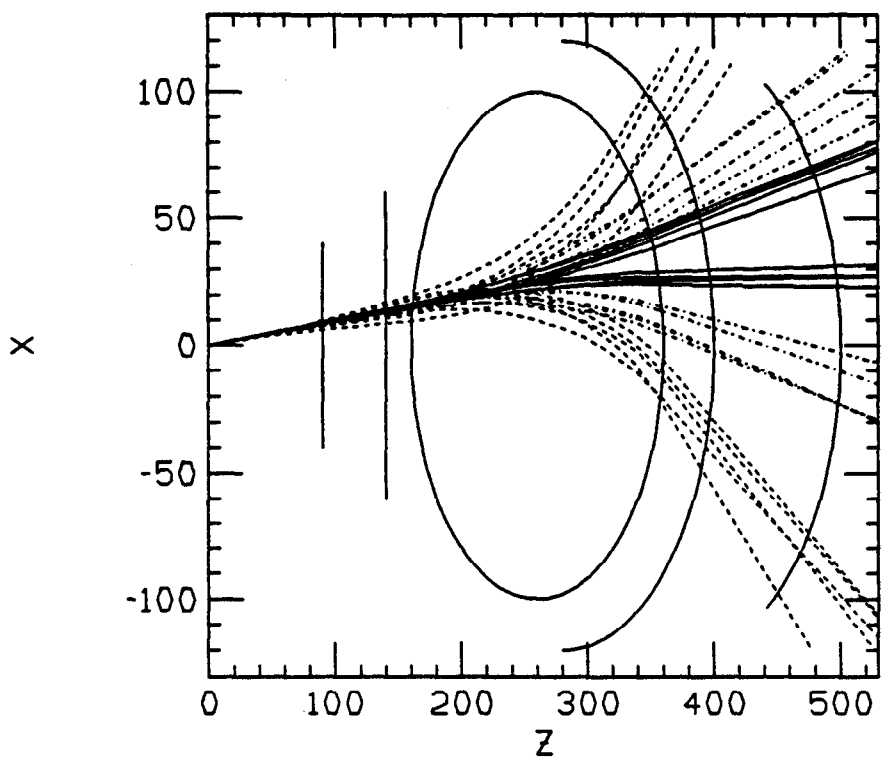

FIG. 18. Ray-trace of muons with momenta of 5 GeV/c (dashed lines), 8 GeV/c (dash-dot), and 15 GeV/c (solid lines), all leaving the target at an angle of 100 mr. For each momentum, there are five μ^+ and five μ^-. The ellipse shows the magnetized iron, while the lines show the detector positions.